Lagrangian modeling of mixing-limited reactive transport in porous media

Guillem Sole-Mari[1,2], **Daniel Fernàndez-Garcia**[1,2], **Xavier Sanchez-Vila**[1,2], **Diogo Bolster**[3]

[1]Department of Civil and Environmental Engineering (DECA), Universitat Politècnica de Catalunya, Barcelona, Spain
[2]Hydrogeology Group (GHS), UPC-CSIC, Barcelona, Spain
[3]Department of Civil and Environmental Engineering and Earth Sciences, University of Notre Dame, South Bend IN, USA

Key Points:

- Development of a new approach to reactive transport modeling that accounts for the dynamics of small-scale concentration fluctuations
- The temporal evolution of integrated mixing metrics agrees with the characteristic trends of fully-resolved systems
- Experimental observations of mixing-limited reactive transport are successfully reproduced

Corresponding author: Guillem Sole-Mari, guillem.sole.mari@upc.edu

Abstract
The presence of solute concentration fluctuations at spatial scales much below the working scale is a major challenge for modeling reactive transport in porous media. Overlooking small-scale fluctuations, which is the usual procedure, often results in strong disagreements between field observations and model predictions, including, but not limited to, the overestimation of effective reaction rates. Existing innovative approaches that account for local reactant segregation do not provide a general mathematical formulation for the generation, transport and decay of these fluctuations and their impact on chemical reactions. We propose a Lagrangian formulation based on the random motion of fluid particles whose departure from the local mean concentration is relaxed through multi-rate interaction by exchange with the mean (MRIEM). We derive and analyze the macroscopic description of the local concentration covariance that emerges from the model and show that mixing-limited processes can be properly simulated. The action of hydrodynamic dispersion on coarse-scale concentration gradients is responsible for the production of local concentration covariance, whereas covariance destruction stems from the local mixing process represented by the MRIEM formulation. The temporal evolution of integrated mixing metrics in two simple scenarios shows the trends that characterize fully-resolved physical systems, such as a late-time power-law decay of the relative importance of incomplete mixing with respect to the total mixing. Experimental observations of mixing-limited reactive transport are successfully reproduced by the model.

1 Introduction

The inherent difficulty of properly representing the interaction of reactive chemicals occurring over multiple spatio-temporal scales in complex hydrodynamic settings renders reactive transport modeling in porous media a major challenge in subsurface hydrology [*Dentz et al.*, 2011; *Sanchez-Vila and Fernàndez-Garcia*, 2016; *Benson et al.*, 2017; *Valocchi et al.*, 2019]. With the exception of highly idealized settings or incredibly small samples, generally in porous media it is unfeasible to obtain a completely resolved flow field within real porous media geometries based on the complete microscopic equations (e.g. Navier-Stokes). This in turn limits the resolution at which a transport model can be applied. Instead one typically describes the system with macroscopic equations in an equivalent continuum [*Icardi et al.*, 2019, and references therein]. By doing so, one essentially ignores detailed resolution of local velocity and concentration fluctuations occurring at the pore-scale, below the scale of the equivalent continuum. The system is represented by macroscopic variables and properties, which aim to represent subscale fluctuations in an effective manner, obtained for instance by volume averaging [*Quintard and Whitaker*, 1994; *Whitaker*, 1999; *Wood et al.*, 2003]. However, these effective parameters really only aim to capture mean behaviors and processes that depend nonlinearly on subscale fluctuations may often not be well described. Similarly, since macroscopic properties such as the hydraulic conductivity can vary substantially in space within real aquifers, one may further upscale flow and transport in heterogeneous media with a new set of effective parameters [*Dagan*, 1989; *Gelhar*, 1993; *Rubin*, 2003]. This step further reduces the apparent complexity of the system, but again does not contain potentially important information below the scale of the effective model.

Among available macroscopic models, the upscaled advection-dispersion-reaction equation (ADRE) is the most widely used for modeling reactive transport at all practical spatial scales. It is embedded as the standard in most popular reactive transport codes [e.g., *Cederberg et al.*, 1985; *Mangold and Tsang*, 1991; *Yeh and Tripathi*, 1991; *Steefel and Lasaga*, 1994; *Walter et al.*, 1994; *Saaltink et al.*, 2004; *De Simoni et al.*, 2005; *Bea et al.*, 2009; *Steefel et al.*, 2015, and references therein]. However, field and laboratory observations, numerical simulations and theoretical developments have demonstrated time and time again that the upscaled ADRE fails to adequately represent mixing and chemical reactions at all scales [*Rashidi et al.*, 1996; *Cao and Kitanidis*, 1998; *Gramling et al.*,

2002; *Palanichamy et al.*, 2009; *Tartakovsky et al.*, 2008; *Fernàndez-Garcia et al.*, 2008; *Edery et al.*, 2009; *Sanchez-Vila et al.*, 2010; *de Anna et al.*, 2014a,b; *Porta et al.*, 2016], because of its disregard for the local concentration fluctuations and the use of scale-averaged concentrations to compute reactions. In fact, the main reason why reaction rates observed in the field tend to be much lower than those measured in laboratory experiments is the presence of anti-correlated local fluctuations of reactant concentrations [*Chiogna and Bellin*, 2013; *Ding et al.*, 2017].

Hence, in order to obtain better predictions, effective transport models should somehow incorporate the sub-scale mixing limitation effects. Several such approaches have been proposed in recent years, both from the Eulerian and from the Lagrangian perspective (see *Porta et al.* [2016] and references therein). The Eulerian approaches are typically restricted to very specific initial and boundary conditions, corresponding to the mixing of two reactants moving across a column-shaped porous medium, forming a sharp interface at $t = 0$, as in the famous laboratory experiments of *Gramling et al.* [2002]. As such, existing effective solutions typically contain a time-decaying term controlling either an apparent kinetic reaction rate [*Sanchez-Vila et al.*, 2010], a pre-defined concentration covariance function [*Chiogna and Bellin*, 2013], or a mobile-mobile mass exchange rate coefficient [*Ginn*, 2018]. *Hochstetler and Kitanidis* [2013] consider a constant, Damkohler-dependent efficiency term multiplying the reaction rate, which accounts for the effect of reactant segregation. While all the above-mentioned approaches provide interesting simplified interpretations of the physical process, they do not provide general differential equations governing the transport of local concentration fluctuations, and hence they might not be applicable to broader sets of initial and boundary conditions. On the other hand, Lagrangian approaches that have been proposed to reproduce mixing-limited reactive transport [*Edery et al.*, 2009; *Ding et al.*, 2013; *Benson et al.*, 2019a] rely on finite particle number effects to emulate the segregation of reactants. While such approaches are equivalent to assuming a noisy initial condition [*Paster et al.*, 2013, 2014], it is difficult to formalize and generalize them in a rigorous manner [*Bolster et al.*, 2016].

Here we present a novel Lagrangian approach to simultaneously account for (*i*) coarse-scale advective-dispersive behavior as well as (*ii*) the generation, transport and decay of local concentration fluctuations. The model aims to offer not just a solution specific to one setting, but rather a mathematical framework to potentially represent a broad array of settings and transport problems. Unlike the aforementioned Lagrangian approaches, the proposed model does not rely on low particle numbers to represent reactant segregation, but in fact converges to the desired solution with sufficient particles (i.e., the particle number is only a numerical discretization). In fact, Eulerian implementations of the proposed model are possible, but Lagrangian implementation is currently more natural and straightforward.

The paper is structured as follows. In §2 we develop the conceptual and mathematical model leading to the differential equation describing the local concentration fluctuations perceived by a random-walking Lagrangian particle. In §3 we derive the resulting Eulerian differential equation describing the transport, generation and decay of concentration point-covariance; we also provide the temporal evolution of the spatial integral of the former (or *mixing state*) in two simple cases of initial and boundary conditions with pseudo-analytical solution. In §4 we implement the proposed model to reproduce the reaction product concentration data corresponding to the laboratory experiments of *Gramling et al.* [2002]. Finally, in §5 we summarize our main conclusions.

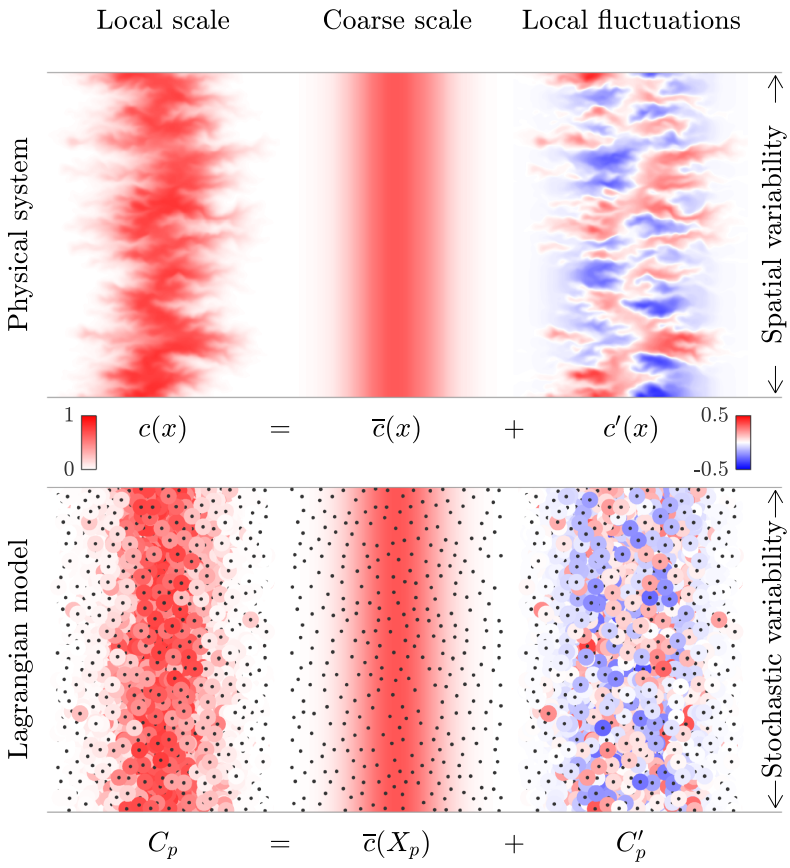

Figure 1. Local concentration variability within a true physical system and its conceptual representation in the proposed Lagrangian model, in which the coarse-scale concentrations are defined on the Eulerian space whereas the local concentrations are defined on the Lagrangian particles. Particles are represented by dark dots, and the colored circles around them show the corresponding local concentrations.

2 Conceptual and mathematical model

2.1 Conservative transport and mixing

By definition, all continuum-scale models of transport in porous media assume or solve a flow field with some degree of coarse-graining; that is, the velocity variability below some threshold resolution is removed and replaced by an upscaled dispersion tensor. We distinguish two spatial scales, above and below this aforementioned threshold, which hereafter we refer to as *coarse scale* and *local scale*, respectively. Coarse-scale concentrations of species A at position $\mathbf{x}$ and time t, $\overline{c}_{\mathrm{A}}(\mathbf{x}, t)$, are often assumed to obey the upscaled advection-dispersion equation,

$$\frac{\partial \overline{c}_{\mathrm{A}}}{\partial t} = \mathcal{L}(\overline{c}_{\mathrm{A}}; \mathbf{v}, \mathbf{D}), \qquad \mathcal{L}(u; \mathbf{v}, \mathbf{D}) \coloneqq \nabla \cdot (-\mathbf{v}u + \mathbf{D}\nabla u) \tag{1}$$

where $\mathbf{v}$ is the coarse-scale velocity, and $\mathbf{D}$ is the dispersion tensor, which represents the combined effect of velocity fluctuations at the local scale (around $\mathbf{v}$) and molecular diffusion. (1) assumes that the porosity (volume of fluid per unit volume of medium) is constant. Hereafter, we also assume that $\mathbf{v}$ and $\mathbf{D}$ are spatially and temporally constant. These assumptions simplify the presentation and analysis of the model, but generalization should be readily possible.

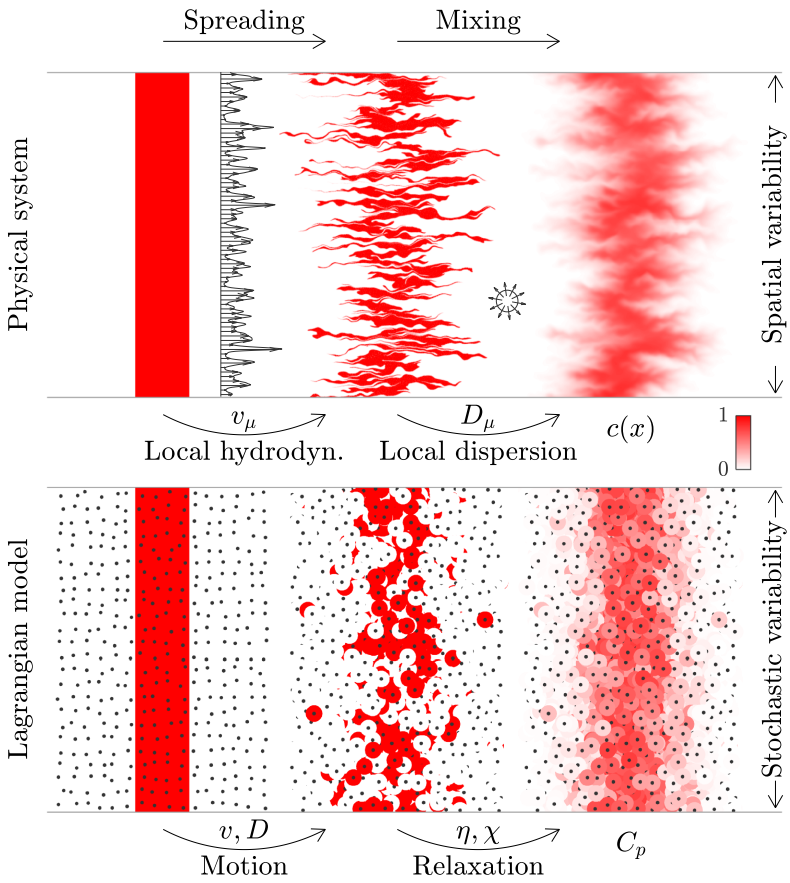

Figure 2. Spreading and mixing within a true physical system and their conceptual representation in the proposed Lagrangian model, in which the coarse-scale transport is simulated by the random motion of particles (2), and the local concentration is updated through multi-rate interaction by exchange with the mean (9). Particles are represented by dark dots, and the colored circles around them show the corresponding local concentrations or fluctuations.

One manner for solving equation (1) is via Random Walk Particle Tracking (RWPT) [e.g., *Salamon et al.*, 2006], a Lagrangian approach in which particles $p = 1, \ldots, N$ carry solute mass of one or several chemical species, and their trajectory over small time intervals $[t, t + \Delta t]$ is defined as a combination of deterministic advective displacements and a Wiener random process emulating dispersion,

$$\mathbf{X}_p\,(t + \Delta t) = \mathbf{X}_p\,(t) + \mathbf{v}\Delta t + \mathbf{B}\boldsymbol{\xi}\sqrt{\Delta t}, \tag{2}$$

where $\mathbf{X}_p$ is the position of particle p, $\mathbf{B}$ is a matrix such that $\mathbf{B}\mathbf{B}^{\mathrm{T}} = \mathbf{D}$, and $\boldsymbol{\xi}$ is a vector of random numbers drawn independently from a standard normal distribution. Here, similar to *Benson and Bolster* [2016a] and *Engdahl et al.* [2017], each particle p is assigned a static mass of solvent, m_p, and a variable concentration of solute A, $C_{\mathrm{A},p}$; therefore the mass of A carried by p is $m_p C_{\mathrm{A},p}$.

Given any particle attribute Ψ_p, one may define its interpolation onto the Eulerian space [*Monaghan*, 2005], here referred to as *local average* (since the interpolation removes any localized variability), at any point $\mathbf{x}$ in model domain Ω^d, where d is the number of spatial dimensions,

$$\langle\Psi\rangle(\mathbf{x}) \coloneqq \sum_p \frac{m_p}{\rho(\mathbf{X}_p)}\Psi_p\delta(\mathbf{x} - \mathbf{X}_p), \tag{3}$$

$$\rho(\mathbf{x}) \coloneqq \sum_p m_p \delta(\mathbf{x} - \mathbf{X}_p), \tag{4}$$

where summation is implied over all particles $p = 1, \ldots, N$, and $\delta(\mathbf{x})$ is the d-dimensional Dirac delta function. Expression (3) is simply a weighted average of Ψ_p over particles p located at $\mathbf{X}_p = \mathbf{x}$; however, this interpretation of the interpolated concentrations is not smooth, other than in the limit of $N \to \infty$, and in practice it must be replaced by some form of small-volume average, for instance by replacing δ in (3) by a kernel function W with nonzero support volume. More details are given in Appendix A: . For

$$\overline{c}_\mathrm{A}(\mathbf{x}, t) \coloneqq \langle C_\mathrm{A}(t) \rangle(\mathbf{x}), \tag{5}$$

given particle motion equation (2) and in the limit $N \to \infty$, $\Delta t \to 0$, the *averaged concentrations* $\overline{c}_\mathrm{A}(\mathbf{x}, t)$ converge to being governed by the Fokker-Planck equation [*Risken*, 1989], which is equivalent to the ADE (1) when $\mathbf{D}$ is spatially constant; otherwise a correction can be applied to the drift term, see *LaBolle et al.* [1996].

To summarize, in the proposed Lagrangian model, each numerical particle represents a discrete amount of a chemical solution traveling through a porous medium, moving by displacements representing the scale-averaged advection (deterministic) and upscaled dispersion (normal random). Consequently, at the coarse scale, the concentration field obeys the advection-dispersion equation (ADE). This type of Lagrangian model is widely used by researchers and practitioners in hydrology to simulate nonreactive transport of solutes.

While coarse-scale concentrations of non-reactive chemicals may agree reasonably well with the ADE under certain conditions [*Dagan*, 1984], concentration fluctuations may still occur at the local scale. These local-scale fluctuations, which are not explicitly accounted for in classical formulations, may drive the outcome of nonlinear processes, such as chemical reactions, far from what would be predicted by the ADE [*Kang et al.*, 2019]. Note that by using equation (2) (or similar stochastic formulations), where each particle follows its own unique random path, it is implied that at any given time each particle is only sampling a portion of the local-scale fluid velocity field. Analogously, in the proposed model, particle concentrations $C_{\mathrm{A},p}(t)$ are assumed to represent the local-scale concentrations, and may therefore be at disequilibrium with the averaged $\overline{c}_\mathrm{A}(\mathbf{x}, t)$. Hence, hereafter we refer to $C_{\mathrm{A},p}(t)$ as *local concentrations*. Figure 1 is a schematic representation that illustrates our proposed conceptual model. The local-scale structured spatial variability of concentrations in the physical system is emulated by the stochastic variability of local concentrations experienced by overlapping Lagrangian particles in the model. Because it is defined by interpolation (see Appendix A:), the coarse-scale concentration is a smooth function in the Eulerian space, whereas local departures from the well-mixed equilibrium or *local fluctuations* are only defined on the Lagrangian particles. In order to represent the evolution of these local fluctuations we need to define a *mixing model*.

A simple representation of the local mixing as seen by a particle p could be to assume a Fickian process driven by a local diffusion D_μ within a fluctuation structure of dimension d_μ and characteristic mixing length ℓ_μ,

$$\frac{\mathrm{d}C_{\mathrm{A},p}}{\mathrm{d}t} = -\frac{\chi}{2}[C_{\mathrm{A},p}(t) - \overline{c}_\mathrm{A}(\mathbf{X}_p(t), t)], \tag{6}$$

where

$$\chi \coloneqq 2 d_\mu D_\mu / \ell_\mu^2 \tag{7}$$

is the mixing rate, which is equal to the inverse time scale for which a typical diffusive displacement matches the characteristic mixing length ℓ_μ. The notation $\mathrm{d}/\mathrm{d}t$ in (6) indicates a *Lagrangian* time-derivative, defined as the temporal variation experienced by a moving fluid particle. This definition is similar to the classical concept of *material* derivative, with the difference that here particles follow stochastic paths instead of pure deterministic advection. The simple model embedded in (6) was originally suggested for mixing in turbulent flows, and it is known as *Interaction by Exchange with the Mean* (IEM)

[*Villermaux*, 1972; *Pope*, 2000]. Its practical numerical implementation requires some careful consideration, related to features such as mass conservation. Implementation aspects, including small-volume approximations of the averaging operator, are discussed in Appendix A: . An appealing advantage of this kind of mixing model is that a local value's variation in time depends only on its current degree of departure from the mean, potentially avoiding direct particle-particle interaction. Importantly in our context, the process is Markovian, i.e., the time-derivative (6) depends only on the current state. We note, however, that equation (6) is overly simplistic. Previous attempts to apply the IEM model (from an Eulerian perspective) to laminar flow and transport in heterogeneous porous media have concluded that, at the beginning of new contact between solutions with different chemical composition, one should account for a growing stage of ℓ_μ before it reaches a stable asymptotic value [*Kapoor and Kitanidis*, 1998; *de Dreuzy et al.*, 2012]. That is, a single constant value of χ cannot reproduce the distinct stages of the mixing process, and one should consider not only a slow linear mixing, but also a fast stretching-enhanced mixing stage. Moreover, fluctuations may occur across multiple overlapping length scales. As acknowledged by *Villermaux* [1983] in the context of IEM applied to turbulent mixing, "several stages for mixing, each with their own time constants should be considered, possibly in series or in parallel". Here, we propose a parallel multi-rate interaction by exchange with the mean (MRIEM), based on representing the mixing process as occurring within different virtual *mixing zones* $i = 1, \ldots, N_Z$, each being sampled by a fraction η_i of the particle ($\sum_i \eta_i = 1$). Within each mixing zone i, each particle p sees a local concentration $C_{A,p,i}(t)$ of each species A, possibly at disequilibrium with $\overline{c}_A(\mathbf{X}_p(t), t)$, such that

$$C_{A,p}(t) = \sum_i \eta_i C_{A,p,i}(t), \tag{8}$$

and

$$\frac{dC_{A,p,i}}{dt} = -\frac{\chi_i}{2}[C_{A,p,i}(t) - \overline{c}_A(\mathbf{X}_p(t), t)]. \tag{9}$$

The values of η_i and χ_i are assumed to depend on local-scale flow and transport conditions. The zone-concentration values $C_{A,p,i}(t)$ do not necessarily have a physical meaning individually, but are instead intended to emulate the complex transient nature of the mixing process. In principle, parameter sets η_i and χ_i can be different for each species to account, for instance, for different values of the local-scale diffusion coefficient.

Given any Lagrangian-defined attribute Ψ_p and its average across the particle space $\langle\Psi\rangle$, it can be shown (see Appendix B:) that, if particles move according to (2), the following relation holds between the Eulerian and the Lagrangian time-derivatives of Ψ:

$$\frac{\partial\langle\Psi\rangle}{\partial t} = \mathcal{L}\left(\langle\Psi\rangle; \mathbf{v}, \mathbf{D}\right) + \left\langle\frac{d\Psi}{dt}\right\rangle. \tag{10}$$

Then, by combining (10) with (8) and (9) we see that

$$\frac{\partial\overline{c}_A}{\partial t} \equiv \frac{\partial\langle C_A\rangle}{\partial t} = \mathcal{L}\left(\overline{c}_A; \mathbf{v}, \mathbf{D}\right). \tag{11}$$

That is, the local mixing process described by (9) does not modify the coarse-scale description of non-reactive transport, driven by the particle displacements in (2).

One of the simplest implementations would comprise only two zones, one of them with an *instantaneous* mixing rate (i.e., very fast in relation to the time scale of interest),

$$1 - \eta_1 = \eta_2 \equiv \eta, \qquad \chi_1 \approx \infty, \qquad \chi_2 \equiv \chi. \tag{12}$$

Hereafter, we refer to this particular case as *dual-rate*, to η as the *slow mixing fraction*, and to χ as the *slow mixing rate*. In this case the local concentration in zone 1 is always at equilibrium with the coarse-scale concentration. Combining equations (8), (9) and (12) we may write:

$$\frac{dC_{A,p}}{dt} = (1-\eta)\frac{d\overline{c}_{A,p}}{dt} - \frac{\chi}{2}[C_{A,p}(t) - \overline{c}_A(\mathbf{X}_p(t), t)], \tag{13}$$

where for conciseness from here on, inside the derivative we use the notation $\overline{c}_{\mathrm{A},p}(t) \equiv \overline{c}_{\mathrm{A}}(\mathbf{X}_p(t), t)$. In the dual-rate model (12), equation (13) can be interpreted as such: While following its random path described by (2), fluid-particle p may experience variations in the perceived coarse-scale concentration of A. Conceptually, these changes correspond to the particle seeing itself involved in new *mixing events*, that is, in the formation of new fluctuation structures. Only a portion $1 - \eta$ of these variations, corresponding to the pre-asymptotic or deformation-related mixing fraction, equilibrates instantaneously with the new coarse-scale concentration. Hence, a local disequilibrium of the opposite sign corresponding to the remaining unmixed fraction η is generated, and it will decay over time following a stationary Fickian mixing process at rate χ.

Figure 2 illustrates the conceptual decoupling of transport as a combination of spreading and mixing, in the true physical system as well as in the proposed Lagrangian model in one coarse-scale dimension. In the physical system, spreading represents the growth of the width (variance) of a solute plume due to velocity variability, which, alone, does not generate new contact between otherwise segregated solute molecules. Mixing, on the other hand, is precisely the generation of new contact between formerly segregated solutes, and is the result of local dispersion applied to the structure generated by spreading (see upper-right part of Figure 2). This decoupled picture is a simplification, because there is a continuous interplay between the two processes. The rate of spreading is influenced non-linearly by local dispersion [e.g., *van Milligen and Bons*, 2012]. Similarly, mixing is influenced by the growth of contact surfaces, which is controlled by local advection [e.g., *Villermaux*, 2012]. In the proposed Lagrangian model, spreading is represented by particle motion (2), which controls the coarse-scale behavior of concentrations; mixing is represented by the relaxation equation (9), which mitigates local departures from equilibrium experienced by individual particles, arising due to the aforementioned random motion.

2.2 Reactive transport

The proposed Lagrangian model can be extended to reactive transport applications by following the premise that chemical reactions occur at the local scale and thus are controlled exclusively by local concentrations defined on Lagrangian particles. We provide a brief summary on the incorporation of kinetic transformation (§2.2.1) and equilibrium speciation (§2.2.2). Naturally, the two may be integrated together, such as in *Molins et al.* [2004].

2.2.1 Kinetic reactions

Consider multiple kinetic reactions labeled $k = 1, \dots, N_{\mathrm{R}}$, with reaction rate laws that model reactions as a function of solute concentrations, $r_k(\mathbf{C})$, where $\mathbf{C} \equiv [C_{\mathrm{A}}, C_{\mathrm{B}}, \dots]^{\mathrm{T}}$; and stoichiometric coefficients $\nu_{\mathrm{A},k}, \nu_{\mathrm{B},k}, \dots$, which indicate the generation/consumption of concentration per unit extent of reaction. Equation (9) is then extended to:

$$\frac{\mathrm{d}C_{\mathrm{A},p,i}}{\mathrm{d}t} = -\frac{\chi_i}{2}[C_{\mathrm{A},p,i}(t) - \overline{c}_{\mathrm{A}}(\mathbf{X}_p(t), t)] + \mathcal{R}_{\mathrm{A}}(\mathbf{C}_p(t)) \tag{14}$$

where

$$\mathcal{R}_{\mathrm{A}}(\mathbf{C}) \coloneqq \sum_k \nu_{\mathrm{A},k} r_k(C_{\mathrm{A}}, C_{\mathrm{B}}, \dots). \tag{15}$$

By combining (14) with (10) we obtain the coarse-scale Eulerian description

$$\frac{\partial \overline{c}_{\mathrm{A}}}{\partial t} = \mathcal{L}(\overline{c}_{\mathrm{A}}; \mathbf{v}, \mathbf{D}) + \langle \mathcal{R}_{\mathrm{A}}(\mathbf{C}) \rangle. \tag{16}$$

Equation (16) elucidates that, for nonlinear reaction systems, i.e., $\langle \mathcal{R}_{\mathrm{A}}(\mathbf{C}) \rangle \neq \mathcal{R}_{\mathrm{A}}(\overline{\mathbf{c}})$, the Eulerian description of reactive transport does not obey the classical form of the advection-dispersion-reaction equation (ADRE) where reactions are computed directly from averaged concentrations. This is in contrast with the conservative transport case, where as shown by equation (11), coarse-scale concentrations do follow the classical ADE.

2.2.2 *Equilibrium reactions*

In the case of equilibrium reactions, a common approach is to compute the transport of chemically conservative components [e.g., *Saaltink et al.*, 1998; *Molins et al.*, 2004; *De Simoni et al.*, 2005], and then speciation is provided by solving equilibrium system,

$$C_{\mathrm{A},p}(t) = \mathcal{E}_{\mathrm{A}}(\mathbf{U}_p(t)). \tag{17}$$

where $\mathcal{E}_{\mathrm{A}}(\mathbf{U})$ combines the law of mass action and the different stoichiometries to find the equilibrium concentrations, from components $\mathbf{U} \equiv \{U_{\mathrm{A}}, U_{\mathrm{B}}, \dots\}$. In (17), $\mathbf{U}_p$ follow the conservative transport and mixing model presented in §2.1. By taking the particle average on both sides of (17), we obtain the coarse-scale description of the equilibrium reaction system

$$\overline{c}_{\mathrm{A}} = \langle \mathcal{E}_{\mathrm{A}}(\mathbf{U}) \rangle. \tag{18}$$

We note from (18) that, similar to the kinetic reaction example, $\overline{c}_{\mathrm{A}} \neq \mathcal{E}_{\mathrm{A}}(\overline{\mathbf{u}})$, as opposed to classical well-mixed reactive transport approaches.

3 Covariance of fluctuations

Here we study the behavior of the local concentration fluctuations, in terms of the local concentration co-variance of two chemically conservative compounds A and B (where the particular single-compound case is implicitly included as A ≡ B). First, in §3.1, we derive the partial differential equation describing covariance generation, transport and destruction. Then, in §3.2, we study integrated mixing metrics for two specific cases with closed form solutions.

3.1 Governing equation

By defining the local fluctuation as the departure from well-mixed equilibrium on particles,

$$C'_{\mathrm{A},p}(t) \coloneqq C_{\mathrm{A},p}(t) - \overline{c}_{\mathrm{A}}(\mathbf{X}_p(t), t) = \sum_i \eta_i C'_{\mathrm{A},p,i}(t), \tag{19}$$

$$C'_{\mathrm{A},p,i}(t) \coloneqq C_{\mathrm{A},p,i}(t) - \overline{c}_{\mathrm{A}}(\mathbf{X}_p(t), t), \tag{20}$$

one may rewrite equation (9) as

$$\frac{\mathrm{d}C'_{\mathrm{A},p,i}}{\mathrm{d}t} = -\frac{\mathrm{d}\overline{c}_{\mathrm{A},p}}{\mathrm{d}t} - \frac{\chi_i}{2} C'_{\mathrm{A},p,i}(t). \tag{21}$$

By definition, $\langle C'_{\mathrm{A}} \rangle(\mathbf{x}, t) = 0$. We study the concentration covariance of species A and B, which we denote as $\Sigma_{\mathrm{AB}}(\mathbf{x}, t)$,

$$\Sigma_{\mathrm{AB}} \coloneqq \langle C'_{\mathrm{A}} C'_{\mathrm{B}} \rangle = \sum_{i,j} \hat{\eta}_{ij} \langle C'_{\mathrm{A},i} C'_{\mathrm{B},j} \rangle \equiv \sum_{i,j} \hat{\eta}_{ij} \Sigma_{\mathrm{AB},ij}, \qquad \hat{\eta}_{ij} \coloneqq \eta_i \eta_j. \tag{22}$$

As noted in §2.1, the assumption that the mixing dynamics of A and B can be described by the same sets of parameters $\{\eta_1, \dots, \eta_{N_{\mathrm{Z}}}\}$, $\{\chi_1, \dots, \chi_{N_{\mathrm{Z}}}\}$, is made here only for the sake of simplicity, and this assumption could be relaxed.

For a particle p, following a first-order integration of equation (21) over a small time step $[t, t + \Delta t]$, we have

$$\begin{aligned} C'_{\mathrm{A},p,i}(t + \Delta t)\, C'_{\mathrm{B},p,j}(t + \Delta t) = &\left(C'_{\mathrm{A},p,i}(t) - \left[\overline{c}_{\mathrm{A},p}(t + \Delta t) - \overline{c}_{\mathrm{A},p}(t) \right] - \frac{\chi_i}{2} \Delta t\, C'_{\mathrm{A},p,i}(t) \right) \\ &\times \left(C'_{\mathrm{B},p,j}(t) - \left[\overline{c}_{\mathrm{B},p}(t + \Delta t) - \overline{c}_{\mathrm{B},p}(t) \right] - \frac{\chi_j}{2} \Delta t\, C'_{\mathrm{B},p,j}(t) \right). \end{aligned} \tag{23}$$

For $\chi\Delta t \ll 1$, this can be rewritten as

$$\Delta(C'_{\mathrm{A},p,i}C'_{\mathrm{B},p,j}) = \Delta\overline{c}_{\mathrm{A},p}\Delta\overline{c}_{\mathrm{B},p} - \hat{\chi}_{ij}\Delta t C'_{\mathrm{A},p,i}C'_{\mathrm{B},p,j} - \left(C'_{\mathrm{A},p,i}\Delta\overline{c}_{\mathrm{B},p} + C'_{\mathrm{B},p,j}\Delta\overline{c}_{\mathrm{A},p}\right), \tag{24}$$

with ΔU denoting the variaton of U in time step Δt, and

$$\hat{\chi}_{ij} \coloneqq \frac{\chi_i + \chi_j}{2}. \tag{25}$$

The first-order Taylor expansion of $\Delta\overline{c}_{\mathrm{A},p}$ is

$$\begin{aligned}\Delta\overline{c}_{\mathrm{A},p} &\approx \Delta\mathbf{X}_p^{\mathrm{T}}\nabla\overline{c}_{\mathrm{A}} + \Delta t\frac{\partial\overline{c}_{\mathrm{A}}}{\partial t} = \sqrt{2\Delta t}\,\boldsymbol{\xi}^{\mathrm{T}}\mathbf{B}^{\mathrm{T}}\nabla\overline{c}_{\mathrm{A}} + \Delta t\left[\mathbf{v}^{\mathrm{T}}\nabla\overline{c}_{\mathrm{A}} + \mathcal{L}(\overline{c}_{\mathrm{A}};\mathbf{v},\mathbf{D})\right] \\ &= \sqrt{2\Delta t}\,\boldsymbol{\xi}^{\mathrm{T}}\mathbf{B}^{\mathrm{T}}\nabla\overline{c}_{\mathrm{A}} + \Delta t\,\nabla\cdot(\mathbf{D}\nabla c_{\mathrm{A}}) \approx \sqrt{2\Delta t}\,\boldsymbol{\xi}^{\mathrm{T}}\mathbf{B}^{\mathrm{T}}\nabla\overline{c}_{\mathrm{A}}.\end{aligned} \tag{26}$$

Note that in the last step of (26) we keep the lower-order term only. Considering the analogous expression for $\Delta\overline{c}_{\mathrm{B},p}$, we may rewrite (24) as

$$\Delta(C'_{\mathrm{A},p,i}C'_{\mathrm{B},p,j}) = 2\Delta t\nabla\overline{c}_{\mathrm{A}}^{\mathrm{T}}\mathbf{B}\boldsymbol{\xi}\boldsymbol{\xi}^{\mathrm{T}}\mathbf{B}^{\mathrm{T}}\nabla\overline{c}_{\mathrm{B}} - \hat{\chi}_{ij}\Delta t C'_{\mathrm{A},p,i}C'_{\mathrm{B},p,j} - \left(C'_{\mathrm{A},p,i}\Delta\overline{c}_{\mathrm{B},p} + C'_{\mathrm{B},p,j}\Delta\overline{c}_{\mathrm{A},p}\right). \tag{27}$$

Dividing both sides of (27) by Δt, taking the limit of $\Delta t \to 0$, and taking the expected value, we obtain:

$$\left\langle\frac{\mathrm{d}(C'_{\mathrm{A},i}C'_{\mathrm{B},j})}{\mathrm{d}t}\right\rangle = 2\nabla\overline{c}_{\mathrm{A}}^{\mathrm{T}}\mathbf{D}\nabla\overline{c}_{\mathrm{B}} - \hat{\chi}_{ij}\langle C'_{\mathrm{A},i}C'_{\mathrm{B},j}\rangle. \tag{28}$$

Finally, substituting into equation (10),

$$\frac{\partial\Sigma_{\mathrm{AB},ij}}{\partial t} = 2\nabla\overline{c}_{\mathrm{A}}^{\mathrm{T}}\mathbf{D}\nabla\overline{c}_{\mathrm{B}} - \hat{\chi}_{ij}\Sigma_{\mathrm{AB},ij} + \mathcal{L}(\Sigma_{\mathrm{AB},ij};\mathbf{v},\mathbf{D}). \tag{29}$$

We have obtained the partial differential equation describing the spatio-temporal evolution of the "ij" entry of the local concentration covariance of A and B in the absence of reactions. The total local concentration covariance can be then obtained as the sum of all entries, as indicated by (22). Let us consider, once again, the specific case represented by (12). Then, one may write:

$$\frac{\partial\Sigma_{\mathrm{AB}}}{\partial t} = 2\eta^2\nabla\overline{c}_{\mathrm{A}}^{\mathrm{T}}\mathbf{D}\nabla\overline{c}_{\mathrm{B}} - \chi\Sigma_{\mathrm{AB}} + \mathcal{L}(\Sigma_{\mathrm{AB}};\mathbf{v},\mathbf{D}). \tag{30}$$

It is worth remarking that, for B = A, expression (30) is mathematically equivalent to the *concentration variance conservation equation* introduced by *Kapoor and Gelhar* [1994, equation 56], provided a scalar proportionality in their proposed dual-dispersivity system such that η fulfills $\mathbf{A} = \eta^2(\boldsymbol{\alpha} + \mathbf{A})$, where $\boldsymbol{\alpha}$ and $\mathbf{A}$ are the microdispersivity and macrodispersivity tensors, respectively. Hence, the two conceptual models have clear similarities since in our case η is the fraction of non-instantaneous mixing, and in *Kapoor and Gelhar* [1994], by analogy, it is the square root of the fraction of total dispersivity that is attributed to the macrodispersivity, i.e., to the non-mixed spreading. Nevertheless, there are important nuances that distinguish the models, as will be discussed in §4.2.

In any case, determining concentration variance/covariance is not the main, or at least not the only, purpose of our model. As outlined in §2.2, the distribution of local concentrations represented by the particles affects local processes such as chemical reactions. Nevertheless, the concentration covariance is a powerful tool to assess contact between solutions, and therefore a good proxy for the potential magnitude of incomplete mixing effects on chemical reactions.

3.2 Mixing state evolution

This section focuses on the dual-rate (fast/slow) local mixing parametrization (12). The results are elementary building blocks for other more complex cases. The differential equation (30) is linked with the solution of (1) through the source term

$$S(\mathbf{x},t) \coloneqq 2\eta^2\nabla\overline{c}_{\mathrm{A}}^{\mathrm{T}}\mathbf{D}\nabla\overline{c}_{\mathrm{B}}. \tag{31}$$

The other terms are exponential decay, advection, and dispersion. Therefore, if $S(\mathbf{x}, t)$ is known, $\Sigma_{\mathrm{AB}}(\mathbf{x}, 0) = 0$, and the domain is unbounded, the solution for the point-covariance evolution can be obtained through the space-time convolution of the Greens function with the source term, i.e.:

$$\Sigma_{\mathrm{AB}}(\mathbf{x}, t) = \int_0^t \int_{\mathbb{R}^d} G\left(\mathbf{x} - \boldsymbol{\kappa}, t - \tau\right) S\left(\boldsymbol{\kappa}, \tau\right) d\boldsymbol{\kappa} \mathrm{d}\tau, \tag{32}$$

with

$$G(\mathbf{x}, t) \coloneqq \left([2\pi]^d 2|\mathbf{D}|t\right)^{-\frac{1}{2}} \exp\left(-\frac{[\mathbf{x} - \mathbf{v}t]^{\mathrm{T}} \mathbf{D}^{-1} [\mathbf{x} - \mathbf{v}t]}{4t} - \chi t\right), \tag{33}$$

where the operator $|\ |$ applied to a tensor is its determinant. A metric that is commonly used to characterize spatial fluctuations of solute concentrations is the so-called mixing state [*Bolster et al.*, 2011; *de Dreuzy et al.*, 2012], which is defined as the spatial integral of the squared concentrations. Here we extend this definition, for any two solutes, A and B, as the spatial integral of the product of the two concentrations. In the present two-scale context, this may be written as

$$M_{\mathrm{AB}}(t) \coloneqq \int_{\Omega^d} \langle C_{\mathrm{A}} C_{\mathrm{B}} \rangle \, \mathrm{d}\mathbf{x} = M^{\overline{\mathrm{c}}}_{\mathrm{AB}}(t) + M^{\Sigma}_{\mathrm{AB}}(t), \tag{34}$$

where Ω^d is the model domain, M_{AB} is the mixing state, $M^{\overline{\mathrm{c}}}_{\mathrm{AB}}$ is the *ideal* mixing when sub-scale fluctuations are not considered, and M^{Σ}_{AB} is the contribution of the local fluctuations to the mixing state (which may be either positive or negative):

$$M^{\overline{\mathrm{c}}}_{\mathrm{AB}}(t) \coloneqq \int_{\Omega^d} \overline{c}_{\mathrm{A}}(\mathbf{x}, t) \overline{c}_{\mathrm{B}}(\mathbf{x}, t) \, \mathrm{d}\mathbf{x}, \qquad M^{\Sigma}_{\mathrm{AB}}(t) \coloneqq \int_{\Omega^d} \Sigma_{\mathrm{AB}}(\mathbf{x}, t) \, \mathrm{d}\mathbf{x}. \tag{35}$$

In the particular case A = B one recovers the classical definition. Additionally, we also quantify the relative deviation from the ideal *well-mixed* behavior:

$$\gamma_{\mathrm{AB}}(t) \coloneqq \frac{M_{\mathrm{AB}} - M^{\overline{\mathrm{c}}}_{\mathrm{AB}}}{M^{\overline{\mathrm{c}}}_{\mathrm{AB}}} = \frac{M^{\Sigma}_{\mathrm{AB}}}{M^{\overline{\mathrm{c}}}_{\mathrm{AB}}}. \tag{36}$$

Here, quantity $\gamma_{\mathrm{AB}}(t)$ is analogous to the $\gamma(t)$ from *de Dreuzy et al.* [2012] for a single species.

In some cases with simple boundary and initial conditions, closed-form solutions exist for the integrals in (35). Below, we provide and discuss two such simple but representative cases.

3.2.1 Continuous injection

Consider a mean-uniform stationary flow in an infinitely long domain, which at the coarse scale can be considered as one-dimensional. At $t = 0$, the concentrations of two solutes A and B are represented by Heaviside-step functions, forming a sharp interface at $x = 0$:

$$\overline{c}_{\mathrm{A}}(x, 0) = c_{\mathrm{o}} \mathcal{H}(-x), \qquad \overline{c}_{\mathrm{B}}(x, 0) = c_{\mathrm{o}} \mathcal{H}(x), \tag{37}$$

where $\mathcal{H}(x)$ is the Heaviside step function. Additionally, $\Sigma_{\mathrm{AB}}(x, 0) = 0$.

The solution of the ADE (1) in this case is

$$\overline{c}_{\mathrm{A}}(x, t) = c_{\mathrm{o}} - \overline{c}_{\mathrm{B}}(x, t) = \frac{c_{\mathrm{o}}}{2} \mathrm{erfc}\left(\frac{x - vt}{2\sqrt{Dt}}\right). \tag{38}$$

Then, the ideal mixing term is

$$M^{\overline{\mathrm{c}}}_{\mathrm{AB}}(t) = \int_{-\infty}^{\infty} \overline{c}_{\mathrm{A}}(x, t) \overline{c}_{\mathrm{B}}(x, t) \, \mathrm{d}x = \pi^{-\frac{1}{2}} c_{\mathrm{o}}^2 \sqrt{2Dt} \equiv \pi^{-\frac{1}{2}} c_{\mathrm{o}}^2 \ell \sqrt{\chi t}, \tag{39}$$

with the characteristic *coarse-scale mixing length* ℓ, defined as

$$\ell \coloneqq \sqrt{2D/\chi}, \tag{40}$$

which is the typical distance traveled by the solute by dispersion within one characteristic mixing time.

For this case, the source term of the covariance (eq. (31)) is:

$$S(x,t) = -\frac{\eta^2 c_o^2 \, \mathrm{e}^{-\frac{(x-vt)^2}{2Dt}}}{2\pi t}, \tag{41}$$

and then the covariance, obtained through equation (32), is

$$\Sigma_{AB}(x,t) = -\frac{\eta^2 c_o^2}{2\pi} \int_0^t [\tau(2t-\tau)]^{-\frac{1}{2}} \exp\left(-\frac{(x-vt)^2}{2D(2t-\tau)} - \chi(t-\tau)\right) \mathrm{d}\tau. \tag{42}$$

To our knowledge, the resulting time-integral in (42) does not have an exact analytical solution. Nevertheless, a (pseudo-)closed form does exist for its integral in space (i.e., the local mixing term):

$$M^{\Sigma}_{AB}(t) = \int_{-\infty}^{\infty} \Sigma_{AB}(x,t)\,\mathrm{d}x = -\pi^{-\frac{1}{2}} \eta^2 c_o^2 \sqrt{\frac{2D}{\chi}}\, F\left(\sqrt{\chi t}\right) \equiv -\pi^{-\frac{1}{2}} \eta^2 c_o^2 \ell\, F\left(\sqrt{\chi t}\right), \tag{43}$$

where $F(u)$ is the Dawson integral:

$$F(u) \coloneqq \mathrm{e}^{-u^2} \int_0^u \mathrm{e}^{r^2} \mathrm{d}r \approx \begin{cases} u, & \text{for } u \ll 1, \\ \frac{1}{2}u^{-1}, & \text{for } u \gg 1. \end{cases} \tag{44}$$

From (43) and (44), we see that there is an early-time regime where concentration covariance generation dominates ($M^{\Sigma}_{AB} \propto t^{1/2}$) followed by a late-time regime where concentration covariance destruction dominates ($M^{\Sigma}_{AB} \propto t^{-1/2}$). M^{Σ}_{AB} is negative meaning that the local covariance reduces the contact between A and B with respect to the ideal value $M^{\bar{c}}_{AB}$. The maximum negative magnitude of $M^{\Sigma}_{AB}(t)$ is achieved for $t = 0.854\chi^{-1}$.

We study the relative deviation from ideal "well-mixed" behavior through γ_{AB} (eq. (36)). From (39) and (43)

$$\gamma_{AB}(t) = \eta^2 \gamma^*_{AB}(\chi t), \tag{45}$$

$$\gamma^*_{AB}(t^*) \coloneqq -\frac{1}{\sqrt{t^*}} F\left(\sqrt{t^*}\right), \tag{46}$$

where $t^* \coloneqq \chi t$ is a dimensionless time.

Figure 3 shows the evolution in time of the mixing metrics. Higher values of the slow-mixing fraction η in the dual-rate model accentuate the departure of the actual mixing state (continuous lines) from the ideal well-mixed case (dotted line). The relative difference between these two quantities, quantified by $\gamma_{AB} = \eta^2 \gamma^*_{AB}$, is highest at the beginning, and decays for $\chi t \gg 1$ as t^{-1}, as can be observed on the log-log scale plot. The actual mixing scales with $t^{1/2}$ for $\chi t \gg 1$. Taking the modeled mixing state M_{AB}, depicted in Figure 3(b), as a proxy for the amount of reaction, we see that it does reproduce trends observed in mixing-limited systems such as simple Poiseuille flows [e.g., *Perez et al.*, 2019, Figure 7].

As outlined at the beginning of §3.2, the summation in (22) allows us generalize the solution for any choice of mixing parameters as a summation of elementary solutions given by (46):

$$\gamma_{AB}(t) = \sum_{i,j} \hat{\eta}_{ij} \gamma^*_{AB}(\hat{\chi}_{ij} t). \tag{47}$$

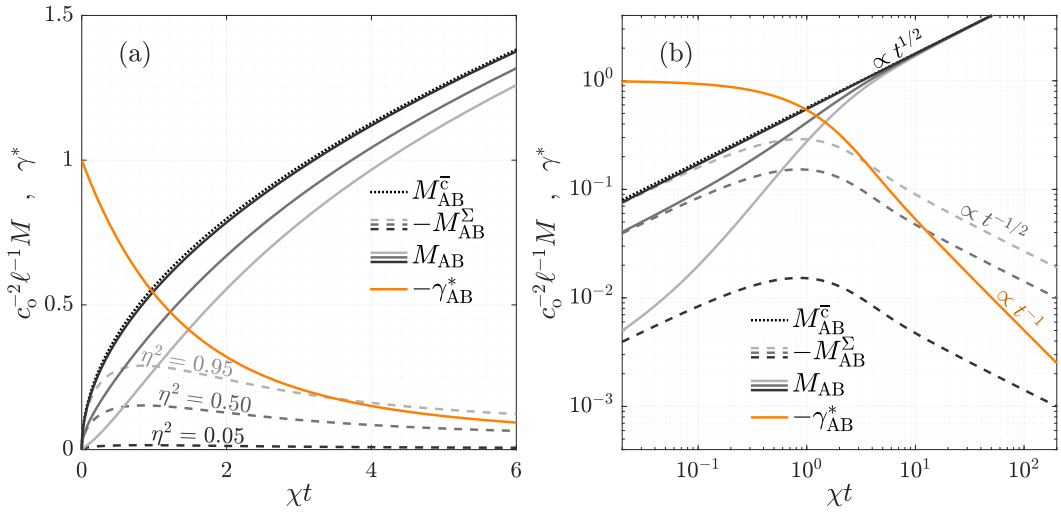

Figure 3. Temporal evolution of various mixing metrics for the dual-rate model (12), according to the solution of equations (1) and (30), for two solutes A and B initially forming a sharp interface perpendicular to the flow direction, shown in (a) linear and (b) logarithmic scale.

3.2.2 Pulse injection

Now let us consider the same simple uniform flow in an infinite-length medium, but with a different initial condition. In this case, there is only one solute A, of which a mass (per cross-section unit area) m_o is injected over a small region around the origin with a Gaussian distribution characterized by a length λ_o:

$$\overline{c}_A(x,0) = \frac{m_o}{\sqrt{2\pi}\lambda_o} e^{-\frac{x^2}{2\lambda_o^2}}. \tag{48}$$

Here we study the mixing state of A, $M_{AA}(t)$. Note that it has the opposite intuitive meaning than the $M_{AB}(t)$ analyzed in §3.2.1: A more advanced mixing process will be characterized by lower values of $M_{AA}(t)$, and viceversa. Once again, we assume that the initial condition for the fluctuations is $\Sigma_{AA}(x,0) = 0$.

The resulting time-dependent mean-concentration profile is also a Gaussian:

$$\overline{c}_A(x,t) = \frac{m_o}{2\sqrt{\pi D(t+t_o)}} e^{-\frac{(x-vt)^2}{4D(t+t_o)}}, \tag{49}$$

with $t_o := \lambda_o^2/2D$. Then, the ideal mixing term is

$$M^{\bar{c}}_{AA}(t) = \int_{-\infty}^{\infty} \overline{c}_A^2(x,t)\,dx = \frac{m_o^2}{\sqrt{8\pi D(t+t_o)}} \equiv \frac{m_o^2}{2\ell\sqrt{\pi\chi(t+t_o)}}. \tag{50}$$

Here, the source term of the variance (eq. (31) with B = A) is:

$$S(x,t) = 2\eta^2 D\left(\frac{\partial \overline{c}_A}{\partial x}\right)^2 = \frac{\eta^2 m_o^2 (x-vt)^2}{8\pi D^2 (t+t_o)^3} e^{-\frac{(x-vt)^2}{2D(t+t_o)}}, \tag{51}$$

and expression (32) gives the evolution of the variance:

$$\Sigma_{AA}(x,t) = \frac{\eta^2 m_o^2}{8\pi D^2}\int_0^t \frac{2D(t-\tau)(2t-\tau+t_o)+(x-vt)^2(\tau+t_o)}{(2t-\tau+t_o)^{2.5}(\tau+t_o)^{1.5}} \times \exp\left(-\frac{(x-vt)^2}{2D(2t-\tau+t_o)} - \chi(t-\tau)\right) d\tau. \tag{52}$$

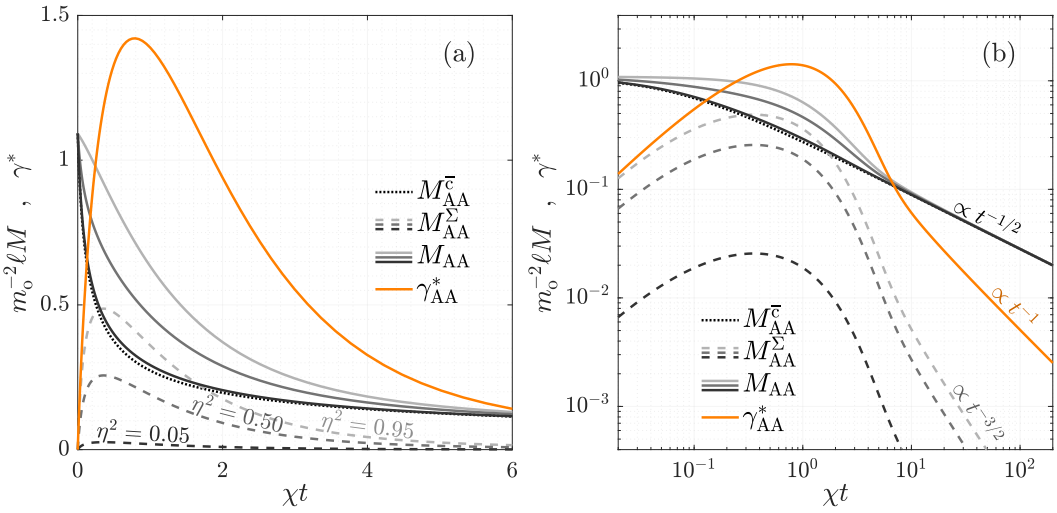

Figure 4. Temporal evolution of various mixing metrics for the dual-rate model (12), according to the solution of equations (1) and (30), for one solute A initially placed as a Gaussian pulse of longitudinal standard deviation 0.26ℓ, shown in (a) linear and (b) logarithmic scale.

Like in the continuous injection case (42), we could not find a closed-form solution to the time-integral in (52). But again, its spatial integral (the local mixing term) can be expressed in terms of the Dawson function (or more precisely, its derivative):

$$M^{\Sigma}_{AA}(t) = \int_{-\infty}^{\infty} \Sigma_{AA}(x,t)\,\mathrm{d}x = \frac{\eta^2 m_o^2}{\sqrt{8\pi D(t+t_o)}}\left[f\left(\sqrt{\chi t_o}\right)\left(\sqrt{1+t/t_o}\right)\mathrm{e}^{-\chi t} - f\left(\sqrt{\chi(t+t_o)}\right)\right]$$
$$\equiv \frac{\eta^2 m_o^2}{2\ell\sqrt{\pi\chi(t+t_o)}}\left[f\left(\sqrt{\chi t_o}\right)\left(\sqrt{1+t/t_o}\right)\mathrm{e}^{-\chi t} - f\left(\sqrt{\chi(t+t_o)}\right)\right], \tag{53}$$

with $f(u)$ defined as the derivative of $F(u)$,

$$f(u) \coloneqq \frac{\mathrm{d}F}{\mathrm{d}u} = 1 - 2u\,F(u) \approx \begin{cases} 1, & \text{for } u \ll 1, \\ -\frac{1}{2}u^{-2}, & \text{for } u \gg 1. \end{cases} \tag{54}$$

Once again, we characterize the relative deviation from the well-mixed behavior:

$$\gamma_{AA}(t) \coloneqq \frac{M^{\Sigma}_{AA}}{M^{\bar{c}}_{AA}} = \eta^2 \gamma^*_{AA}(\chi t; \chi t_o), \tag{55}$$

$$\gamma^*_{AA}(t^*; t^*_o) \coloneqq f\left(\sqrt{t^*_o}\right)\left(\sqrt{1+t^*/t^*_o}\right)\mathrm{e}^{-t^*} - f\left(\sqrt{t^*+t^*_o}\right), \tag{56}$$

with $t^*_o \coloneqq \chi t_o$.

Figure 4 depicts the evolution of the mixing metrics in dimensionless time, for a small value of initial pulse size, with $t_o = (15\chi)^{-1}$. Similar to the case in §3.2.1, higher values of η result in reduced mixing, as exhibited here by higher values of the actual mixing state (continuous lines) compared to the ideal mixing state (dotted line). The ratio between these two quantities, $\gamma_{AA} = \eta^2\gamma^*_{AA}$, is zero at $t = 0$, since there is no incomplete mixing, and it starts to grow as the spreading process generates local concentration fluctuations. This increasing trend peaks at $\chi t \approx 0.785$ (for the specific value of $\chi t_o = 1/15$). After that, fluctuation destruction dominates and γ_{AA} decreases as t^{-1} for $\chi t \gg 1$. At these long times, the actual mixing tends to approach the $\propto t^{-1/2}$ trend of ideal mixing.

These features agree with semi-analytical [*Bolster et al.*, 2011] and numerical [*de Dreuzy et al.*, 2012] calculations of the mixing state evolution in fully-resolved porous media flows for a pulse injection of solute.

As in §3.2.1, elementary solution (56) is a building block for generalizing (55) to more complex mixing parametrizations than the dual-rate form:

$$\gamma_{\mathrm{AA}}(t) = \sum_{i,j} \hat{\eta}_{ij} \gamma^*_{\mathrm{AA}}(\hat{\chi}_{ij} t; \hat{\chi}_{ij} t_{\mathrm{o}}). \tag{57}$$

4 Reproducing results of a reactive transport experiment

4.1 Experimental setup and background

In this Section we use the proposed model to reproduce results from the now well known experiments of *Gramling et al.* [2002]. In these experiments, performed in a column with a saturated granular material, a solution of $EDTA^{4-}$, initially occupying all the pore space with concentration c_{o}, was displaced longitudinally by an invading solution of $CuSO_4$ with the same molar concentration c_{o}. As these two solutes moved through the porous medium, the combination of hydrodynamic dispersion and molecular diffusion allowed them to mix and react forming $CuEDTA^{2-}$, among other reaction products. Hereafter, for simplicity and consistency with the original work, we refer to the three cited compounds as A, B, and AB, respectively. The reaction can be expressed as

$$\mathrm{A} + \mathrm{B} \rightleftharpoons \mathrm{AB}, \tag{58}$$

with equilibrium equation,

$$k_{\mathrm{eq}} \coloneqq \frac{c_{\mathrm{A}} c_{\mathrm{B}}}{c_{\mathrm{AB}}} \ll 1, \tag{59}$$

and a reaction rate that can be assumed instantaneous given the time scales of the experiment. Because equilibrium constant k_{eq} is very small (practically zero), c_{A} and c_{B} will always be instantaneously consumed when in contact, until one of them is exhausted locally (i.e., they cannot coexist). Hence, if we define the following conservative components,

$$u_{\mathrm{A}} \coloneqq c_{\mathrm{A}} + c_{\mathrm{AB}}, \qquad u_{\mathrm{B}} \coloneqq c_{\mathrm{B}} + c_{\mathrm{AB}}, \tag{60}$$

then the reaction product concentration will be given by

$$c_{\mathrm{AB}} = \mathcal{E}_{\mathrm{AB}}(u_{\mathrm{A}}, u_{\mathrm{B}}) = \min\left(u_{\mathrm{A}}, u_{\mathrm{B}}\right). \tag{61}$$

The fully-resolved (pore-scale) transport of u_{A} and u_{B} follows the conservative form of the advection-diffusion equation,

$$\frac{\partial u_{\mathrm{A}}}{\partial t} = \mathcal{L}(u_{\mathrm{A}}; \mathbf{v}_\mu, D_\mu), \tag{62}$$

with operator $\mathcal{L}$ defined as in (1), $\mathbf{v}_\mu$ being the heterogeneous velocity field within the saturated pore geometry, and D_μ being the molecular diffusion coefficient. The analogous of (62) applies to u_{B}; however, in this particular case, because of the initial condition, $u_{\mathrm{A}}(\mathbf{x}, t) + u_{\mathrm{B}}(\mathbf{x}, t) = c_{\mathrm{o}}$, hence we have that $u_{\mathrm{B}}(\mathbf{x}, t) = c_{\mathrm{o}} - u_{\mathrm{A}}(\mathbf{x}, t)$ and the transport is fully described by just one of the two equilibrium components.

However, in practice, a simple and complete solution is rarely obtainable, because of (*i*) the lack of detailed information on the pore geometry and (*ii*) high computational demands, which is why this problem requires an upscaled approach. As an approximation, we ignore the boundary effect at the inlet, i.e., we assume an infinite medium. Then, the upscaled one-dimensional description of the transport of $\overline{u}_{\mathrm{A}}$ and $\overline{u}_{\mathrm{B}}$, under the assumption of Fickian hydrodynamic dispersion, is identical to (38),

$$\overline{u}_{\mathrm{A}}(x, t) = c_{\mathrm{o}} - \overline{u}_{\mathrm{B}}(x, t) = \frac{c_{\mathrm{o}}}{2} \mathrm{erfc}\left(\frac{x - vt}{2\sqrt{Dt}}\right), \tag{63}$$

where the constants v and D are the cross-section averaged vertical velocity and the upscaled longitudinal hydrodynamic dispersion coefficient, respectively. These constants were quantified by the authors of the cited experiment as $v = 1.21 \times 10^{-2}$ cm/s and $D = 1.75 \times 10^{-3}$ cm^2/s. In the classical well-mixed upscaled ADRE approach, in which coarse-scale concentrations govern the chemical reactions, the combination of (63) with (61) would lead to the following equation for the concentration of AB:

$$\overline{c}_{\mathrm{AB}}(x,t) = \frac{c_{\mathrm{o}}}{2}\mathrm{erfc}\left(\frac{|x-vt|}{2\sqrt{Dt}}\right). \tag{64}$$

However, the experimental observations of *Gramling et al.* [2002] do not agree with (64). Instead, the latter tends to overestimate the amount of reaction product generation, because of the incorrectness of the underlying assumption of full local mixing.

4.2 Model implementation and results

The proposed Lagrangian model is implemented as follows. Particles carry local concentrations of just one of the two conservative components, $U_{\mathrm{A},p}(t)$, because the other is defined by $U_{\mathrm{B},p}(t) = 1 - U_{\mathrm{A},p}(t)$. Equal volumes (weights) are assigned to $N = 10^6$ particles, which are initially distributed in space uniformly over an interval $[-L/2, L/2]$, with $L = 15$ cm, and

$$U_{\mathrm{A},p}(0) = \mathcal{H}(-X_p(0)). \tag{65}$$

As detailed in §2.1, transport and mixing of $U_{\mathrm{A},p}(t)$ are decoupled and reproduced by equations (2) and (9), respectively. In the latter, the local averaging operator is implemented through *binning* (see Appendix A:), with a bin size $L/300$. We use a simple dual-rate mixing model like (12), parameterized by a slow mixing fraction η and a slow mixing rate χ. Note that one does not need to explicitly simulate the evolution of the local concentration fraction corresponding to the fast mixing zone, $U_{\mathrm{A},p,1}(t)$, which is always in equilibrium with the average at $X_p(t)$. The coarse-scale reaction product concentration is given by the combination of (61) and (18),

$$\overline{c}_{\mathrm{AB}}(x,t) = \langle \min(U_{\mathrm{A}}(t), U_{\mathrm{B}}(t)) \rangle(x) = \frac{c_{\mathrm{o}}}{2} + \left\langle \left| \frac{c_{\mathrm{o}}}{2} - U_{\mathrm{A}}(t) \right| \right\rangle(x). \tag{66}$$

The code implementing this is written in Matlab (version 2016b) and the simulation runs in less than 5 minutes on a conventional laptop computer (Intel® Core™ i7-6700HQ, 2.60GHz).

An alternative approach to implement the proposed model is also tested, which we refer to as the Eulerian approach since it does not require to explicitly simulate the Lagrangian particles. In this specific case, we have an analytical solution for $\overline{u}_{\mathrm{A}}(x,t) = 1 - \overline{u}_{\mathrm{B}}(x,t)$, given by (63), as well as a semi-analytical solution for $\Sigma_{\mathrm{AB}}(x,t) = -\Sigma_{\mathrm{AA}}(x,t) = -\Sigma_{\mathrm{BB}}(x,t)$, given by (42). These quantities are, in fact, entries of the mean and the covariance matrix of a bivariate distribution (i.e., probability density function) of local concentrations of components A and B at any (coarse-scale) position and time, $\mathcal{F}(U_{\mathrm{A}}, U_{\mathrm{B}}, x, t)$. By assuming that $\mathcal{F}$ is multiGaussian, it is then fully defined by its mean and covariance matrix, and the local average (66) becomes

$$\begin{aligned} \overline{c}_{\mathrm{AB}}(x,t) &= \int_0^{c_{\mathrm{o}}} \int_0^{c_{\mathrm{o}}} \min(U_{\mathrm{A}}, U_{\mathrm{B}}) \mathcal{F}(U_{\mathrm{A}}, U_{\mathrm{B}}, x, t) \mathrm{d}U_{\mathrm{A}} \mathrm{d}U_{\mathrm{B}} \\ &= \frac{c_{\mathrm{o}}}{2} - \sqrt{\frac{2\Sigma_{\mathrm{AA}}}{\pi}} \exp\left(-\frac{(c_{\mathrm{o}}/2 - \overline{u}_{\mathrm{A}})^2}{2\Sigma_{\mathrm{AA}}}\right) - (c_{\mathrm{o}}/2 - \overline{u}_{\mathrm{A}}) \,\mathrm{erf}\left(\frac{c_{\mathrm{o}}/2 - \overline{u}_{\mathrm{A}}}{\sqrt{2\Sigma_{\mathrm{AA}}}}\right), \end{aligned} \tag{67}$$

where we use equation (63) for $\overline{u}_{\mathrm{A}}$ and the numerical time-integration of (42) for $\Sigma_{\mathrm{AA}} = -\Sigma_{\mathrm{AB}}$. Note that the multiGaussianity assumption may introduce inaccuracies, including the fact that a portion of $\mathcal{F}$ may fall outside the physically meaningful interval $[0, c_{\mathrm{o}}]$.

Similar to *Sanchez-Vila et al.* [2010], the dispersion coefficient is set to $D = 1.3 \times 10^{-3}$ cm^2/s, slightly lower than the value of $D = 1.75 \times 10^{-3}$ cm^2/s estimated by *Gramling*

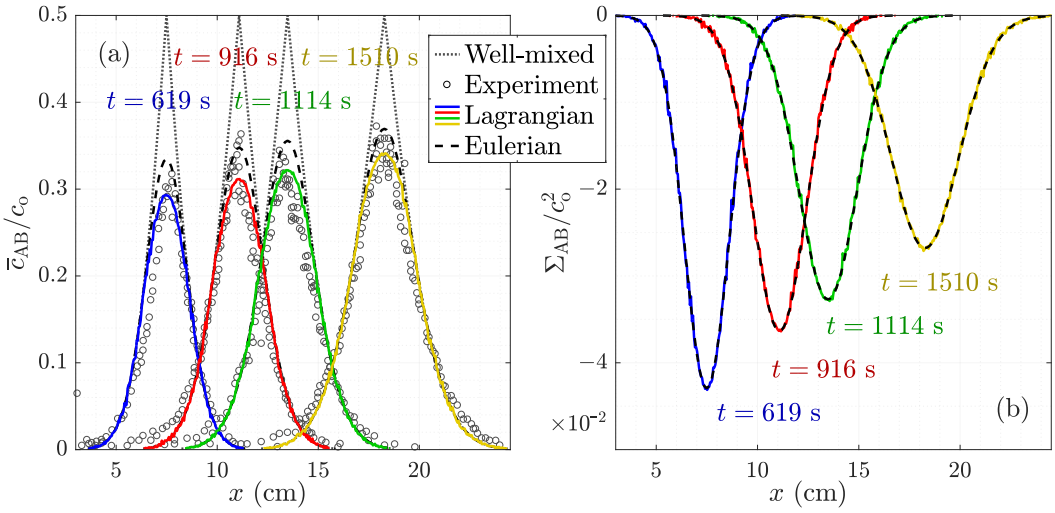

Figure 5. (a) Comparison of various models' predictions of reaction product coarse-scale concentration, $\overline{c}_{AB}$, to the experimental observations of *Gramling et al.* [2002], at four different times, and (b) corresponding point-covariance of U_A and U_B, Σ_{AB}. The local mixing model is given by (9) and (12), with $\eta = 0.5$ and $\chi = 10^{-3}$ s^{-1}. The curves labeled as *Lagrangian* correspond to small-volume average (66) performed on particles in a Lagrangian simulation, whereas the curves labeled as *Eulerian* are drawn using equations (42), (63) and (67). The curves labeled as *Well-mixed* correspond to equation (64).

et al. [2002] from the results of non-reactive experiments. The results of the Lagrangian approach display close agreement with the experimental observations, as shown in Figure 5(a), for manually-adjusted values $\eta = 0.5$ and $\chi = 10^{-3}$ s^{-1}. A possible interpretation is that in the pore-scale flow and transport conditions of the experiment, pre-asymptotic fast mixing controlled about half of the mixing process, whereas diffusive mixing across stable fluctuation structures was responsible for the other half. Assuming that the latter is essentially two-dimensional (dominated by transverse diffusion between concentration filaments), and approximating both reactants' bulk diffusion coefficients as the value for AB reported by the authors of the experiment, $D_\mu = 7.02 \times 10^{-7}$ cm/s, then according to (7),

$$\ell_\mu = \sqrt{4 D_\mu / \chi} = 0.53 \text{ cm} \approx 0.4b, \tag{68}$$

where $b = 0.13$ cm is the mean grain size of the granular medium. That is, ℓ_μ is approximately the typical size of a pore, considering the reported porosity of 0.36. This suggests that the slow mixing process captured by the model corresponds indeed to the diffusive relaxation of pore-scale concentration fluctuations. The inferred value of $\eta = 0.5$ shows that a single-rate local mixing model (i.e, $\eta = 1$) would not be able to reproduce the experimental results. Neither would the high value of $\eta = \sqrt{1 - D_\mu/D} \approx 1$ that would render our model's local covariance behavior equivalent to *Kapoor and Gelhar* [1994] (see discussion below equation (30)). This is consistent with previous studies on mixing in porous media, both at pore and Darcy scales [e.g., *Kapoor and Kitanidis*, 1998; *de Anna et al.*, 2014b; *Le Borgne et al.*, 2013, 2015], which show that, after first encounter between two solutions with different composition, the mixing rate is higher at the beginning and decreases with time. In other words, the dynamics of mixing are subjected to aging, a feature which is effectively reproduced in our model by a parallel multi-rate process (9), without introducing any time-dependent parameters. Although the dual-rate simplification appears to capture the general behavior for this case-study, allowing us to reproduce the experimental results, more complicated forms may be needed depending on the characteristics of the

flow field, especially for highly heterogeneous porous media. This should be the subject of future research and as future experimental datasets in such settings become available.

Looking closely at Figure 5, the main discrepancy between the data and the well-mixed solution (64) is the notable decrease in the peak of reaction product concentrations at the coarse-scale mixing interface. In the Lagrangian simulation, this reduction is caused by the anti-correlated fluctuations of $U_{\mathrm{A},p}$ and $U_{\mathrm{B},p}$ on particles with respect to the local average, which is also reflected by the negative values of Σ_{AB}, depicted in Figure 5(b). As expected, the spatiotemporal description of the covariance in the Eulerian and in the Lagrangian approach are identical, which ratifies the validity of the expressions given in §3.1. However, the reaction product concentration prediction is slightly different, because of the multiGaussian approximation used in the Eulerian approach.

5 Summary and conclusions

We have proposed a Lagrangian mathematical model to represent the transport and mixing of solutes in a dual-scale (coarse/local) framework. Local concentrations carried by individual particles evolve by relaxation towards the coarse-scale concentration values that they perceive along their random path (described by (2)). This relaxation or mixing process is characterized by (9) as a parallel multi-rate *interaction by exchange with the mean* (MRIEM). We derived the differential equation describing the corresponding evolution of the (Eulerian) concentration point-covariance (29), and found solutions corresponding to the mixing state evolution for two simple generic cases. Finally, the proposed model (in its dual-rate form) was successfully implemented to reproduce reaction product concentration data from a well-known laboratory experiment that displays incomplete mixing effects. Below, we enumerate additional findings and conclusions:

1. The partial differential equation describing the behavior of the local concentration covariance becomes nearly equivalent to the *concentration variance conservation equation* suggested by *Kapoor and Gelhar* [1994], given a dual-rate (fast/slow) parametrization of the mixing process.
2. The temporal evolution of the mixing state for a pulse injection shows similar trends to those observed in previous studies of mixing in porous media within fully-resolved systems [*Bolster et al.*, 2011; *de Dreuzy et al.*, 2012], suggesting that the model may be able to accurately upscale local mixing limitations. Both for a pulse and for a continuous injection, the ratio between the mixing state components corresponding to the fluctuating and the averaged concentration terms decays at late times as the inverse of time.
3. The *Gramling et al.* [2002] results would not be explicable, from our model's perspective, through a single-rate local mixing process. This agrees with previous knowledge on the complexity of mixing dynamics in porous media [*de Anna et al.*, 2014b; *Le Borgne et al.*, 2013], which establish the need to somehow include a temporal decrease of the mixing rate from the time of first coarse-scale contact between reactants.
4. Along the same vein, the $\eta = 0.5$ value for the dual-rate model that fits the cited experimental results does not agree with *Kapoor and Gelhar*'s model, that is, with the restriction $\eta^2 = 1 - D_\mu/D \approx 0.9995$, if D_μ is assumed to be the molecular diffusion. This discrepancy can be attributed to the pre-asymptotic stage where mixing is enhanced by fluid deformation dynamics, as noted by *Kapoor and Kitanidis* [1998].
5. Considering the characteristic local mixing distance $\ell_\mu = \sqrt{4D_\mu/\chi}$, the fitted value of $\chi = 10^{-3}$ s^{-1} yields $\ell_\mu \approx 0.05$ cm, which is approximately equal to the typical pore size. This consistency of scale suggests that the model is properly capturing the physics underlying the mixing process.

Several future avenues for research arise due to this work, including (*i*) identifying methods to readily estimate parameter values in (8) and (9) to upscale mixing within different local-scale heterogeneity patterns of velocity and dispersion, thus making the model scalable and translatable to the diverse range of hydrogeologic settings out there (*ii*) exploring the use of motion equations other than (2) [e.g. *Berkowitz et al.*, 2006; *Le Borgne et al.*, 2008], which are well-known to better describe coarse-scale transport in complex heterogeneous settings (*iii*) extending the model to incorporate heterogeneous reactions, and (*iv*) using the model to study the effects of local concentration fluctuations on realistic complex geochemical reaction systems.

A: Aspects of numerical implementation

A.1 Smooth local average

As outlined in §2.1, the numerical implementation of (9), as well as the reactive extensions described in §2.2, entails the definition of a smooth small-volume approximation for the local average operator $\langle\,\rangle(\mathbf{x})$ (equation (3)), which is used to compute the averaged concentrations $\overline{c}_{\mathrm{A}}(\mathbf{x},t)$ from overlapping local concentrations defined on particles. Here we discuss two possible approaches, and their respective advantages and disadvantages.

A.1.1 Binning

A straightforward approach to compute the averaged concentrations is to discretize the spatial domain into a set of bins. The Dirac Delta $\delta(\mathbf{x}-\mathbf{X}_p)$ in (3) and (4) is then replaced by an indicator function $I(\mathbf{x},\mathbf{X}_p)$ that has a value of 1 when $\mathbf{x}$ and $\mathbf{X}_p$ belong to the same bin, and a value of 0 otherwise. Compared to other smoothing techniques, this approach has very low computational demands. Another advantage is that it does not present any mass conservation issues. This is because the sum of all differences with respect to the mean within each individual bin is zero by definition, and therefore so is the sum of all exchanges with the mean given by (9). The main potential disadvantage of binning is that, compared to other smoothing techniques, it tends to require higher particle numbers (here, a finer Lagrangian discretization of the fluid mass) in order to converge to a smooth solution [*Fernàndez-Garcia and Sanchez-Vila*, 2011]. This approach is used in the Lagrangian implementation described in §4.2.

A.1.2 Kernel smoothing

An alternative to binning is to use kernel smoothing on particles, that is, to replace the Dirac Delta $\delta(\mathbf{x}-\mathbf{X}_p)$ in (3) and (4) with a radially symmetric kernel $W(\mathbf{x}-\mathbf{X}_p;h)$, where h is the smoothing bandwidth. This interpolation method is commonly used in smoothed particle hydrodynamics [*Monaghan*, 2005]. This approach may offer better convergence rates with particle number than binning. On the other hand, in this case, exact mass conservation for (9) is not guaranteed by default, and a correction strategy is required. One mass-conserving approach can be obtained by considering symmetric pairwise particle interactions. Let us first define a smooth interpolator to approximate (3) that is pair-wise symmetric

$$\langle\Psi\rangle(\mathbf{x}) \coloneqq \sum_p \frac{m_p}{\tilde{\rho}(\mathbf{x},\mathbf{X}_p)}\Psi_p W(\mathbf{x}-\mathbf{X}_p). \tag{A.1}$$

Here, $\tilde{\rho}(\mathbf{x},\mathbf{X}_p)$ is some average of $\rho(\mathbf{x})$ and $\rho(\mathbf{X}_p)$. We redefine (9) by inserting $C_{\mathrm{A},p,i}$ inside the local average operator

$$\frac{\mathrm{d}C_{\mathrm{A},p,i}}{\mathrm{d}t} = -\frac{\chi_i}{2}\langle C_{\mathrm{A},p,i}-C_{\mathrm{A},i}\rangle(\mathbf{X}_p) = -\frac{\chi_i}{2}\sum_q \frac{m_q}{\tilde{\rho}(\mathbf{X}_q,\mathbf{X}_p)}[C_{\mathrm{A},p,i}-C_{\mathrm{A},q,i}]W(\mathbf{X}_q-\mathbf{X}_p). \tag{A.2}$$

The right-hand side of (A.2) clearly shows that a symmetric and therefore consistent mass exchange between each pair of particles p, q, is imposed [*Herrera et al.*, 2009; *Sole-Mari*

et al., 2019]. This expression may also be rewritten as

$$\frac{\mathrm{d}C_{\mathrm{A},p,i}}{\mathrm{d}t} = -\frac{\chi_i}{2}[C_{\mathrm{A},p,i}\langle 1\rangle(\mathbf{X}_p) - \overline{c}_{\mathrm{A}}(\mathbf{X}_p)], \tag{A.3}$$

which elucidates that mass conservation can be achieved in the kernel-based MRIEM through multiplication of $C_{\mathrm{A},p,i}$ by a correcting factor $\langle 1\rangle(\mathbf{X}_p)$, which converges to 1 as $N \to \infty$ and $h \to 0$. However, this approach does come at higher computational cost than binning.

A.2 Numerical dispersion and relation with other formulations

Smoothing tends to artificially spread out particle masses, which may generate some numerical dispersion in the Lagrangian numerical implementation. This can be straightforwardly quantified by comparing the right-hand side of (A.2) to the SPH formulation used to simulate a diffusion D_{SPH} with a multiGaussian W [*Sole-Mari et al.*, 2019, eq. 8]. Both expressions become equivalent by setting

$$D_{\mathrm{SPH}} = \frac{1}{4}\chi_i h^2. \tag{A.4}$$

That is, the identity (A.4) quantifies the numerical diffusion involved in the numerical simulation of a MRIEM mixing with rate χ_i using a Gaussian smoothing kernel with bandwidth h for computing the averaged concentrations. The same quadratic scaling should be expected for the bin size when binning is the chosen smoothing approach. Fortunately, as explained in §4.2, the high or virtually instantaneous fraction of mixing rates in the MRIEM formulation do not need to be explicitly simulated, and therefore only the small values of χ_i may produce numerical dispersion, which can be controlled by choosing a small-enough smoothing bandwidth h, or by slightly reducing the value of D used in the particle motion such that the added total dispersion has the correct value. The latter strategy, in fact, is tightly related to previous works [*Benson and Bolster*, 2016b; *Herrera et al.*, 2017; *Sole-Mari et al.*, 2019; *Engdahl et al.*, 2019; *Benson et al.*, 2019a,b] in which the total dispersion results from the sum of (*i*) random walks and (*ii*) some form of exchange between particles. In particular, if we look at the approach suggested by *Benson and Bolster* [2016b, eq. 7], with mass transfers based on probabilities of collision between particles, we see that it is equivalent to the kernel form of the MRIEM as given by (A.2) for the specific case of a single mixing zone $i = 1$ with mixing rate $\chi_1 = 1/\mathrm{d}t$, and a multiGaussian W with bandwidth $h^2 = 4D_{\mathrm{MT}}\mathrm{d}t$. That is, the mass transfer approach by *Benson and Bolster* [2016b] is equivalent to a Gaussian kernel-based single-rate IEM with instantaneous full mixing and "numerical" dispersion (see (A.4)) $D_{\mathrm{SPH}} = D_{\mathrm{MT}}$.

B: Relation between local averages of Eulerian and Lagrangian derivatives

In this Appendix we provide the derivation for expression (10) given in §2.1. We start from the definition of local average (3). Note that, for incompressible flow, the fluid density $\rho(\mathbf{X}_p)$ is proportional to the porosity – amount of fluid per unit volume of medium. Hence, maintaining the assumption of constant porosity, the particle estimate of fluid density given by (4) must converge to a constant value ρ as $N \to \infty$, N being the number of particles. The time-derivative of expression (3) is then

$$\frac{\partial\langle\Psi\rangle}{\partial t} = \sum_p \frac{m_p}{\rho}\Psi_p\frac{\mathrm{d}\delta(\mathbf{x}-\mathbf{X}_p)}{\mathrm{d}t} + \sum_p \frac{m_p}{\rho}\frac{\mathrm{d}\Psi_p}{\mathrm{d}t}\delta(\mathbf{x}-\mathbf{X}_p) = \sum_p \frac{m_p}{\rho}\Psi_p\frac{\Delta\delta(\mathbf{x}-\mathbf{X}_p)}{\Delta t} + \Big\langle\frac{\mathrm{d}\Psi}{\mathrm{d}t}\Big\rangle. \tag{B.1}$$

where the time-derivative of the Dirac delta function has been written as the variation $\Delta\delta(\mathbf{x}-\mathbf{X}_p)$ over Δt, where $\Delta t \to 0$. A second-order Taylor expansion over the corresponding small particle displacement $\Delta\mathbf{X}_p$ writes:

$$\Delta\delta(\mathbf{x}-\mathbf{X}_p) \approx \Delta\mathbf{X}_p^{\mathrm{T}}\delta'(\mathbf{x}-\mathbf{X}_p) + \frac{1}{2}\Delta\mathbf{X}_p^{\mathrm{T}}\delta''(\mathbf{x}-\mathbf{X}_p)\Delta\mathbf{X}_p, \tag{B.2}$$

where δ' and δ'' are, respectively, the gradient and the Hessian matrix of δ. Then, using expression (B.2), knowing that the weighted summation is equivalent (in the limit $N \rightarrow \infty$) to an integral over the particle space, and given the evaluation properties of the Dirac delta distributional derivatives, we may rewrite the summation in (B.1) as

$$\begin{aligned}\sum_p \frac{m_p}{\rho}\Psi_p \frac{\Delta\delta(\mathbf{x}-\mathbf{X}_p)}{\Delta t} &\approx \sum_p \frac{m_p}{\rho}\left[-\nabla\cdot\left(\Psi_p\frac{\Delta\mathbf{X}_p}{\Delta t}\right)+\frac{1}{2}\nabla\nabla:\left(\Psi_p\frac{\Delta\mathbf{X}_p^{\mathrm{T}}\Delta\mathbf{X}_p}{\Delta t}\right)\right]\delta(\mathbf{x}-\mathbf{X}_p)\\ &= -\nabla\cdot\langle\Psi_p\frac{\Delta\mathbf{X}_p}{\Delta t}\rangle+\frac{1}{2}\nabla\nabla:\langle\Psi_p\frac{\Delta\mathbf{X}_p^{\mathrm{T}}\Delta\mathbf{X}_p}{\Delta t}\rangle\\ &= -\mathbf{v}\nabla\cdot\langle\Psi_p\rangle+\mathbf{D}\nabla\nabla:\langle\Psi_p\rangle=\mathcal{L}\left(\langle\Psi\rangle;\mathbf{v},\mathbf{D}\right),\end{aligned} \tag{B.3}$$

where we applied well-known identities associated to (2) [*Risken*, 1989; *Salamon et al.*, 2006], $\langle\Delta\mathbf{X}_p\rangle = \mathbf{v}\Delta t$ and $\langle\Delta\mathbf{X}_p^{\mathrm{T}}\Delta\mathbf{X}_p\rangle = 2\mathbf{D}\Delta t$ (for $\Delta t \rightarrow 0$), and assumed that $\mathbf{v}$ and $\mathbf{D}$ are spatially constant. Finally, introducing the result from (B.3) in (B.1), we obtain the expression given by (10),

$$\frac{\partial\langle\Psi\rangle}{\partial t} = \mathcal{L}\left(\langle\Psi\rangle;\mathbf{v},\mathbf{D}\right)+\langle\frac{\mathrm{d}\Psi}{\mathrm{d}t}\rangle, \tag{B.4}$$

which states that the Eulerian temporal variation of $\langle\Psi\rangle$ comprises a contribution from the flux of particles (Fokker-Planck) plus a local contribution from variations on particles.

Acknowledgments

This work was partially supported by the European Comission, through grant H2020-MSCA-ITN-2018; by the Spanish Ministry of Economy and Competitiveness, through grant PCIN-2015-248; by the Spanish Ministry of Science, Innovation and Universities, through grant RTI2018-101990-B-I00; and by the Catalan Agency for Management of University and Research Grants, through grant 2017-SGR-1485. DB and GSM acknowledge financial support by the US Army Research Office under contract/grant number W911NF-18-1-0338. The Matlab script used for the Lagrangian simulation in §4.2 is available on Zenodo (doi:10.5281/zenodo.3588401).

References

Bea, S., J. Carrera, C. Ayora, F. Batlle, and M. Saaltink (2009), Cheproo: A fortran 90 object-oriented module to solve chemical processes in earth science models, *Computers and Geosciences*, *35*(6), 1098–1112, doi:https://doi.org/10.1016/j.cageo.2008.08.010.

Benson, D. A., and D. Bolster (2016a), Arbitrarily complex chemical reactions on particles, *Water Resources Research*, *52*(11), 9190–9200, doi:10.1002/2016WR019368.

Benson, D. A., and D. Bolster (2016b), Arbitrarily Complex Chemical Reactions on Particles, *Water Resources Research*, *52*(11), 1–20, doi:10.1002/2016WR019368.

Benson, D. A., T. Aquino, D. Bolster, N. Engdahl, C. V. Henri, and D. Fernàndez-Garcia (2017), A comparison of Eulerian and Lagrangian transport and non-linear reaction algorithms, *Advances in Water Resources*, *99*, 15–37, doi:10.1016/j.advwatres.2016.11.003.

Benson, D. A., S. Pankavich, and D. Bolster (2019a), On the separate treatment of mixing and spreading by the reactive-particle-tracking algorithm: An example of accurate upscaling of reactive poiseuille flow, *Advances in Water Resources*, *123*, 40 – 53, doi:https://doi.org/10.1016/j.advwatres.2018.11.001.

Benson, D. A., S. Pankavich, M. Schmidt, and G. Sole-Mari (2019b), Entropy: The former trouble with particles (including a new numerical model computational penalty for the akaike information criterion).

Berkowitz, B., A. Cortis, M. Dentz, and H. Scher (2006), Modeling Non-fickian transport in geological formations as a continuous time random walk, *Reviews of Geophysics*, *44*(2), doi:10.1029/2005RG000178.

Bolster, D., F. J. Valdés-Parada, T. LeBorgne, M. Dentz, and J. Carrera (2011), Mixing in confined stratified aquifers, *Journal of Contaminant Hydrology*, *120-121*, 198 – 212,

doi:https://doi.org/10.1016/j.jconhyd.2010.02.003, reactive Transport in the Subsurface: Mixing, Spreading and Reaction in Heterogeneous Media.

Bolster, D., A. Paster, and D. A. Benson (2016), A particle number conserving Lagrangian method for mixing-driven reactive transport, *Water Resources Research*, *52*(2), 1518–1527, doi:10.1002/2015WR018310.

Cao, J., and P. K. Kitanidis (1998), Pore-scale dilution of conservative solutes: An example, *Water Resources Research*, *34*(8), 1941–1949, doi:10.1029/98WR01468.

Cederberg, G. A., R. L. Street, and J. O. Leckie (1985), A groundwater mass transport and equilibrium chemistry model for multicomponent systems, *Water Resources Research*, *21*(8), 1095–1104, doi:10.1029/WR021i008p01095.

Chiogna, G., and A. Bellin (2013), Analytical solution for reactive solute transport considering incomplete mixing within a reference elementary volume, *Water Resources Research*, *49*(5), 2589–2600, doi:10.1002/wrcr.20200.

Dagan, G. (1984), Solute transport in heterogeneous porous formations, *Journal of Fluid Mechanics*, *145*, 151–177, doi:10.1017/S0022112084002858.

Dagan, G. (1989), *Flow and Transport in Porous Formations*, Springer-Verlag.

de Anna, P., J. Jimenez-Martinez, H. Tabuteau, R. Turuban, T. Le Borgne, M. Derrien, and Y. Méheust (2014a), Mixing and reaction kinetics in porous media: An experimental pore scale quantification, *Environmental Science & Technology*, *48*(1), 508–516, doi:10.1021/es403105b, pMID: 24274690.

de Anna, P., M. Dentz, A. Tartakovsky, and T. Le Borgne (2014b), The filamentary structure of mixing fronts and its control on reaction kinetics in porous media flows, *Geophysical Research Letters*, *41*(13), 4586–4593, doi:10.1002/2014GL060068.

de Dreuzy, J.-R., J. Carrera, M. Dentz, and T. Le Borgne (2012), Time evolution of mixing in heterogeneous porous media, *Water Resources Research*, *48*(6), doi:10.1029/2011WR011360.

De Simoni, M., J. Carrera, X. Sánchez-Vila, and A. Guadagnini (2005), A procedure for the solution of multicomponent reactive transport problems, *Water Resources Research*, *41*(11), doi:10.1029/2005WR004056.

Dentz, M., T. Le Borgne, A. Englert, and B. Bijeljic (2011), Mixing, spreading and reaction in heterogeneous media: A brief review, doi:10.1016/j.jconhyd.2010.05.002.

Ding, D., D. A. Benson, A. Paster, and D. Bolster (2013), Modeling bimolecular reactions and transport in porous media via particle tracking, *Advances in Water Resources*, *53*, 56 – 65, doi:https://doi.org/10.1016/j.advwatres.2012.11.001.

Ding, D., D. A. Benson, D. Fernàndez-Garcia, C. V. Henri, D. W. Hyndman, M. S. Phanikumar, and D. Bolster (2017), Elimination of the Reaction Rate "Scale Effect": Application of the Lagrangian Reactive Particle-Tracking Method to Simulate Mixing-Limited, Field-Scale Biodegradation at the Schoolcraft (MI, USA) Site, *Water Resources Research*, *53*(12), 10,411–10,432, doi:10.1002/2017WR021103.

Edery, Y., H. Scher, and B. Berkowitz (2009), Modeling bimolecular reactions and transport in porous media, *Geophysical Research Letters*, *36*(2), n/a–n/a, doi:10.1029/2008GL036381.

Engdahl, N. B., D. A. Benson, and D. Bolster (2017), Lagrangian simulation of mixing and reactions in complex geochemical systems, *Water Resources Research*, *53*(4), 3513–3522, doi:10.1002/2017WR020362.

Engdahl, N. B., M. J. Schmidt, and D. A. Benson (2019), Accelerating and parallelizing lagrangian simulations of mixing-limited reactive transport, *Water Resources Research*, *55*(4), 3556–3566, doi:10.1029/2018WR024361.

Fernàndez-Garcia, D., and X. Sanchez-Vila (2011), Optimal reconstruction of concentrations, gradients and reaction rates from particle distributions, *Journal of Contaminant Hydrology*, *120-121*(C), 99–114, doi:10.1016/j.jconhyd.2010.05.001.

Fernàndez-Garcia, D., X. Sánchez-Vila, and A. Guadagnini (2008), Reaction rates and effective parameters in stratified aquifers, *Advances in Water Resources*, *31*(10), 1364–1376, doi:10.1016/j.advwatres.2008.07.001.

Gelhar, L. W. (1993), *Stochastic Subsurface Hydrology*, Prentice-Hall.

Ginn, T. R. (2018), Modeling bimolecular reactive transport with mixing-limitation: Theory and application to column experiments, *Water Resources Research*, *54*(1), 256–270, doi:10.1002/2017WR022120.

Gramling, C. M., C. F. Harvey, and L. C. Meigs (2002), Reactive Transport in Porous Media: A Comparison of Model Prediction with Laboratory Visualization, *Environmental Science & Technology*, *36*(11), 2508–2514, doi:10.1021/es0157144.

Herrera, P. A., M. Massabó, and R. D. Beckie (2009), A meshless method to simulate solute transport in heterogeneous porous media, *Advances in Water Resources*, *32*(3), 413–429, doi:10.1016/j.advwatres.2008.12.005.

Herrera, P. A., J. M. Cortínez, and A. J. Valocchi (2017), Lagrangian scheme to model subgrid-scale mixing and spreading in heterogeneous porous media, *Water Resources Research*, *53*(4), 3302–3318, doi:10.1002/2016WR019994.

Hochstetler, D. L., and P. K. Kitanidis (2013), The behavior of effective rate constants for bimolecular reactions in an asymptotic transport regime, *Journal of Contaminant Hydrology*, *144*(1), 88 – 98, doi:https://doi.org/10.1016/j.jconhyd.2012.10.002.

Icardi, M., G. Boccardo, and M. Dentz (2019), *Upscaling Flow and Transport Processes*, pp. 137–176, Springer International Publishing, Cham.

Kang, P. K., E. Bresciani, S. An, and S. Lee (2019), Potential impact of pore-scale incomplete mixing on biodegradation in aquifers: From batch experiment to field-scale modeling, *Advances in Water Resources*, *123*, 1 – 11, doi:https://doi.org/10.1016/j.advwatres.2018.10.026.

Kapoor, V., and L. W. Gelhar (1994), Transport in three-dimensionally heterogeneous aquifers: 1. dynamics of concentration fluctuations, *Water Resources Research*, *30*, 1775–1788, doi:10.1029/94WR00076.

Kapoor, V., and P. K. Kitanidis (1998), Concentration fluctuations and dilution in aquifers, *Water Resources Research*, *34*(5), 1181–1193, doi:10.1029/97WR03608.

LaBolle, E. M., G. E. Fogg, and A. F. B. Tompson (1996), Random-walk simulation of transport in heterogeneous porous media: Local mass-conservation problem and implementation methods, *Water Resources Research*, *32*(3), 583–593, doi:10.1029/95WR03528.

Le Borgne, T., M. Dentz, and J. Carrera (2008), Lagrangian statistical model for transport in highly heterogeneous velocity fields, *Phys. Rev. Lett.*, *101*, 090,601, doi:10.1103/PhysRevLett.101.090601.

Le Borgne, T., M. Dentz, and E. Villermaux (2013), Stretching, coalescence, and mixing in porous media, *Phys. Rev. Lett.*, *110*, 204,501, doi:10.1103/PhysRevLett.110.204501.

Le Borgne, T., M. Dentz, and E. Villermaux (2015), The lamellar description of mixing in porous media, *Journal of Fluid Mechanics*, *770*, 458–498, doi:10.1017/jfm.2015.117.

Mangold, D. C., and C.-F. Tsang (1991), A summary of subsurface hydrological and hydrochemical models, *Reviews of Geophysics*, *29*(1), 51–79, doi:10.1029/90RG01715.

Molins, S., J. Carrera, C. Ayora, and M. W. Saaltink (2004), A formulation for decoupling components in reactive transport problems, *Water Resources Research*, *40*(10), doi:10.1029/2003WR002970.

Monaghan, J. J. (2005), Smoothed particle hydrodynamics, *Reports on Progress in Physics*, *68*(8), 1703–1759, doi:10.1088/0034-4885/68/8/r01.

Palanichamy, J., T. Becker, M. Spiller, J. Köngeter, and S. Mohan (2009), Multicomponent reaction modelling using a stochastic algorithm, *Computing and Visualization in Science*, *12*(2), 51–61, doi:10.1007/s00791-007-0080-y.

Paster, A., D. Bolster, and D. A. Benson (2013), Particle tracking and the diffusion-reaction equation, *Water Resources Research*, *49*(1), 1–6, doi:10.1029/2012WR012444.

Paster, A., D. Bolster, and D. A. Benson (2014), Connecting the dots: Semi-analytical and random walk numerical solutions of the diffusion-reaction equation with stochastic initial conditions, *Journal of Computational Physics*, *263*, 91–112, doi:10.1016/j.jcp.2014.01.020.

Perez, L. J., J. J. Hidalgo, and M. Dentz (2019), Upscaling of mixing-limited bimolecular chemical reactions in poiseuille flow, *Water Resources Research*, *55*(1), 249–269, doi: 10.1029/2018WR022730.

Pope, S. B. (2000), *PDF methods*, p. 463–557, Cambridge University Press, doi: 10.1017/CBO9780511840531.014.

Porta, G., G. Ceriotti, and J.-F. Thovert (2016), Comparative assessment of continuum-scale models of bimolecular reactive transport in porous media under pre-asymptotic conditions, *Journal of Contaminant Hydrology*, *185-186*, 1 – 13, doi: https://doi.org/10.1016/j.jconhyd.2015.12.003.

Quintard, M., and S. Whitaker (1994), Transport in ordered and disordered porous media ii: Generalized volume averaging, *Transport in Porous Media*, *14*(2), 179–206, doi: 10.1007/BF00615200.

Rashidi, M., L. Peurrung, A. Tompson, and T. Kulp (1996), Experimental analysis of pore-scale flow and transport in porous media, *Advances in Water Resources*, *19*(3), 163 – 180, doi:https://doi.org/10.1016/0309-1708(95)00048-8.

Risken, H. (1989), *The Fokker-Planck equation. Methods of solution and applications*.

Rubin, Y. (2003), *Applied stochastic hydrogeology*, New York : Oxford University Press.

Saaltink, M. W., C. Ayora, and J. Carrera (1998), A mathematical formulation for reactive transport that eliminates mineral concentrations, *Water Resources Research*, *34*(7), 1649–1656, doi:10.1029/98WR00552.

Saaltink, M. W., F. Batlle, C. Ayora, J. Carrera, and S. Olivella (2004), RETRASO, a code for modeling reactive transport in saturated and unsaturated porous media, *Geologica Acta*, *2*(3), 235–251, doi:10.1344/105.000001430.

Salamon, P., D. Fernàndez-Garcia, and J. J. Gómez-Hernández (2006), A review and numerical assessment of the random walk particle tracking method, *Journal of Contaminant Hydrology*, *87*(3-4), 277–305, doi:10.1016/j.jconhyd.2006.05.005.

Sanchez-Vila, X., and D. Fernàndez-Garcia (2016), Debates-Stochastic subsurface hydrology from theory to practice: Why stochastic modeling has not yet permeated into practitioners?, *Water Resources Research*, *52*(12), 9246–9258, doi:10.1002/2016WR019302.

Sanchez-Vila, X., D. Fernàndez-Garcia, and A. Guadagnini (2010), Interpretation of column experiments of transport of solutes undergoing an irreversible bimolecular reaction using a continuum approximation, *Water Resources Research*, *46*(12), doi: 10.1029/2010WR009539.

Sole-Mari, G., M. J. Schmidt, S. D. Pankavich, and D. A. Benson (2019), Numerical equivalence between sph and probabilistic mass transfer methods for lagrangian simulation of dispersion, *Advances in Water Resources*, *126*, 108 – 115, doi: https://doi.org/10.1016/j.advwatres.2019.02.009.

Steefel, C. I., and A. C. Lasaga (1994), A coupled model for transport of multiple chemical species and kinetic precipitation/dissolution reactions with application to reactive flow in single phase hydrothermal systems, *American Journal of Science*, doi: 10.2475/ajs.294.5.529.

Steefel, C. I., C. A. J. Appelo, B. Arora, D. Jacques, T. Kalbacher, O. Kolditz, V. Lagneau, P. C. Lichtner, K. U. Mayer, J. C. L. Meeussen, S. Molins, D. Moulton, H. Shao, J. Šimůnek, N. Spycher, S. B. Yabusaki, and G. T. Yeh (2015), Reactive transport codes for subsurface environmental simulation, *Computational Geosciences*, *19*(3), 445–478, doi:10.1007/s10596-014-9443-x.

Tartakovsky, A. M., G. Redden, P. C. Lichtner, T. D. Scheibe, and P. Meakin (2008), Mixing-induced precipitation: Experimental study and multiscale numerical analysis, *Water Resources Research*, *44*(6), doi:10.1029/2006WR005725.

Valocchi, A. J., D. Bolster, and C. J. Werth (2019), Mixing-limited reactions in porous media, *Transport in Porous Media*, *130*(1), 157–182, doi:10.1007/s11242-018-1204-1.

van Milligen, B. P., and P. D. Bons (2012), Analytical model for tracer dispersion in porous media, *Phys. Rev. E*, *85*, 011,306, doi:10.1103/PhysRevE.85.011306.

Villermaux, E. (2012), Mixing by porous media, *Comptes Rendus Mécanique*, *340*(11), 933 – 943, doi:https://doi.org/10.1016/j.crme.2012.10.042, out of Equilibrium Dynamics.

Villermaux, J. (1972), Représentation de la coalescence et de la redispersion des domaines de ségrégation dans un fluide par un modèle d'interaction phénoménologique, in *Proceedings of the Second International Symposium on Chemical Reaction Engineering*, pp. 1–13, Elsevier.

Villermaux, J. (1983), Mixing in Chemical Reactors, in *Chemical Reaction Engineering—Plenary Lectures*, *ACS Symposium Series*, vol. 226, pp. 135–186 SE – 6, AMERICAN CHEMICAL SOCIETY, doi:10.1021/bk-1983-0226.ch006.

Walter, A. L., E. O. Frind, D. W. Blowes, C. J. Ptacek, and J. W. Molson (1994), Modeling of multicomponent reactive transport in groundwater: 1. model development and evaluation, *Water Resources Research*, *30*(11), 3137–3148, doi:10.1029/94WR00955.

Whitaker, S. (1999), *The Method of Volume Averaging*, Theory and applications of transport in porous media, Springer.

Wood, B. D., F. Cherblanc, M. Quintard, and S. Whitaker (2003), Volume averaging for determining the effective dispersion tensor: Closure using periodic unit cells and comparison with ensemble averaging, *Water Resources Research*, *39*(8), doi:10.1029/2002WR001723.

Yeh, G.-T., and V. S. Tripathi (1991), A model for simulating transport of reactive multispecies components: Model development and demonstration, *Water Resources Research*, *27*(12), 3075–3094, doi:10.1029/91WR02028.